

NEUTRON ELECTRIC-DIPOLE MOMENT, ULTRACOLD NEUTRONS AND POLARIZED ^3He

R. GOLUB^a and Steve K. LAMOREAUX^b

^a*Hahn–Meitner Institut, Postfach 390128, Glienicker Strasse 100, 14109 Berlin, Germany*

^b*University of Washington, Department of Physics FM-15, Seattle, WA 98195, USA*



NORTH-HOLLAND

Neutron electric-dipole moment, ultracold neutrons and polarized ^3He

R. Golub^a and Steve K. Lamoreaux^b

^a*Hahn–Meitner Institut, Postfach 390128, Glienicke Strasse 100, 14109 Berlin, Germany*

^b*University of Washington, Department of Physics FM-15, Seattle, WA 98195, USA*

Received May 1993; editor: J. Eichler

Contents:

1. Introduction	4	5.3. Solution by use of the secular approximation	38
1.1. Historical background	4	5.4. Elimination of the pseudomagnetic field suppression by feedback to ω_z	39
2. Current experimental technique	8	5.5. Effects of the z component of the pseudomagnetic field	42
2.1. Ultracold neutrons (UCN)	8	5.6. Effects of offsets in the first-harmonic signal	44
2.2. Neutron EDM measurements with stored UCN	10	6. Noise analysis	45
2.3. Recent EDM experiments using UCN	13	6.1. Model of the system for noise analysis	45
3. Superfluid He neutron EDM with ^3He comagnetometer	19	6.2. Initial polarization and UCN density	45
3.1. Introduction	19	6.3. Analysis of harmonically modulated dressing	46
3.2. Production of UCN in superfluid ^4He	20	6.4. Evolution of the UCN polarization and density under modulated dressing	46
3.3. Polarization of UCN	21	6.5. Noise analysis in the feedback system	47
3.4. Polarization of ^3He	22	7. Some technical questions in regard to the proposed experiment	51
3.5. Detection of scintillations	23	7.1. Overview of the experiment	51
3.6. ^3He as a comagnetometer	23	7.2. Operating temperature	52
3.7. Elimination of the effects of the dc magnetic field by means of “critical dressing”	24	7.3. Magnetic-field homogeneity requirements	53
3.8. Application of critical dressing to the search for a neutron EDM	25	7.4. High-voltage considerations	54
4. Quantum analysis of the dressed spin system	26	7.5. Scintillation detection	55
4.1. Constant magnetic field as a perturbation on the eigenstates of the spin in an oscillating field	26	7.6. Sources of cold neutrons	56
4.2. Time dependence of $\langle\sigma\rangle$	28	8. Conclusion	57
4.3. Time dependence of $\sigma_n \cdot \sigma_3$	29	Appendix A. Mathematical operations on the Pauli matrices	57
4.4. Effect of an x -component of the static magnetic field	30	Appendix B. Quantum versus classical behaviour in the ^3He –UCN system	58
4.5. Effect of variation of the static field	30	Appendix C. ^3He distribution in dilute ^3He – ^4He solutions: a new application of neutron beams	59
4.6. Numerical solution of free precession with rf and dc fields	31	References	60
5. Interaction of UCN with ^3He	32		
5.1. Introduction	32		
5.2. Time evolution of the UCN spin with modulated dressing	33		

Abstract:

A brief review of the history of the experimental search for the neutron electric-dipole moment (EDM) is presented, followed by a discussion of the “state of the art” experimental techniques based on the storage of ultracold neutrons. Also discussed is the recent work on the construction of an improved experiment incorporating a ^{199}Hg magnetometer within the ultracold neutron storage volume.

We then review a number of well-known experimental and theoretical results and propose an entirely new experimental technique to search for the neutron EDM based on storing together, in superfluid ^4He , polarized ultracold neutrons and a polarized gas of ^3He atoms; this forms a unique system of two spins interacting by means of a spin-dependent mutual absorption. Such a system appears to be ideally suited for use in a neutron EDM search. Following a brief description of the method, we present an analysis of the dynamics of such a system and calculate the statistical uncertainties to be expected in an EDM search. We show that, in principle, improvement by a factor of over 1000 in the experimental limit is possible. This limit would be more than sufficient to determine whether the known CP violation leads to the observed cosmological baryon asymmetry and, in addition, would set very strict limits on the supersymmetric, multi-Higgs, and left-right-symmetric models of CP violation. We conclude with a discussion of some technical questions related to the proposed experimental technique.

1. Introduction

The electric-dipole moment (EDM) of the neutron has been interesting to physicists since 1950 [Purcell and Ramsey 1950]. Today some 45 years later this interest is significantly stronger although, in all this time, nobody has been able to observe an EDM of the neutron or any other elementary particle. The reason for this lies in the fact that the existence of an EDM for an elementary particle would be direct evidence for the violation of time-reversal symmetry (T violation) as well as parity (P violation). For many years it was accepted as canon that the laws of physics would have to be symmetric under P and T transformations, as the contradiction of this requirement implied that empty space would possess properties such as a preferred direction, and that physical results would not be independent of the coordinate system we choose to describe them. In this paper we present a review of the historical development and the current “state of the art” concerning the neutron EDM. We then go on to describe how a system of polarized Ultra-Cold Neutron (UCN) gas and a polarized gas of ^3He atoms, a unique system of two spins interacting by means of a mutual absorption, is ideally suited for a neutron EDM search. We present an estimate of the accuracy to be expected from such an experiment and conclude with a short discussion of some technical questions.

1.1. Historical background

1.1.1. The Dirac magnetic monopole

For many years all known experimental evidence from atomic and nuclear physics was in agreement with the postulate that the laws of physics are invariant under the P and T symmetry operations. It was Dirac [1949] who first questioned this tenet in print. As early as 1949 he wrote, “I do not believe there is any need for physical laws to be invariant under reflections in space and time although the exact laws of nature so far known do have this invariance.” Dirac was interested in the possible existence of particles with free magnetic charge. This would make Maxwell’s equations more symmetric regarding the interchange of electric and magnetic fields but would violate the P and T symmetries. However, as Dirac [1948, 1949] showed, the existence of magnetic charge would provide a natural explanation for the quantization of electric charge so that the acceptance of P and T violation seemed a reasonable price to pay. Up to the present time all attempts to observe the magnetic monopole have been unsuccessful [Goldhaber and Trower 1990].

1.1.2. The neutron electric-dipole moment (EDM)

The neutron ground state, having spin $I = 1/2$, is completely specified by the spin projection quantum number $m_I = \pm 1/2$. In external electric and magnetic fields \mathbf{E} and \mathbf{B} the Hamiltonian is

$$H = -(d_n \mathbf{I} \cdot \mathbf{E} + \mu_n \mathbf{I} \cdot \mathbf{B})/I, \quad (1.1)$$

where d_n and μ_n are the electric- and magnetic-dipole moments of the neutron [Golub and Pendlebury 1972]. The electric-dipole moment must lie along \mathbf{I} otherwise additional quantum numbers would be necessary to describe the neutron ground state; in addition, any component perpendicular to \mathbf{I} would be unobservable. This Hamiltonian manifests P violation; under

$P, E \rightarrow -E$ and B and I are unchanged; so that the possible existence of a nonzero EDM of an elementary particle was long considered an absurdity by all-right thinking physicists. However in 1950, perhaps inspired by Dirac's speculations, Purcell and Ramsey [1950] suggested that the above arguments against the existence of a neutron EDM are not really compelling and the question of P violation, like all questions in physics, must be addressed experimentally. Indeed, as is now well known, the idea that any physically acceptable Hamiltonian must commute with the parity operator subsequently had to be abandoned. The authors cited Dirac's magnetic charge as a possible physical mechanism that could lead to an EDM. They also argued that since matter in our vicinity of the universe shows an enormous asymmetry with respect to the relative amounts of matter and antimatter, we should accept the possibility of elementary particles appearing asymmetric as a result of possessing a nonzero EDM. Thus the existence or not of an elementary-particle EDM should be investigated experimentally, and such an investigation would also serve as an experimental test of parity conservation. Emboldened by these arguments, they then proceeded to search for a possible EDM of the neutron using a magnetic-resonance technique with a neutron beam. This first experiment to search for a neutron EDM was set on a neutron beam at Oak Ridge and produced the result (in 1951) $d_n = -(0.1 \pm 2.4) \times 10^{-20} e \text{ cm}$ [Smith 1951]. We can get an idea of the attitude of the contemporary physics community to this work by the observation that it was not published for a further six years [Smith et al. 1957].

1.1.3. The τ - θ puzzle and the discovery of parity violation

Lee and Yang [1956] suggested that parity nonconservation could explain the τ - θ puzzle; the fact that two particles, called in those days τ^+ and θ^+ , decayed into states with opposite parities in spite of having the same masses, production rates and lifetimes. These latter observations were strongly suggestive of the two particles being, in fact, different decay modes of one and the same particle. Thus Lee and Yang were led to review the experimental evidence relating to the question of parity conservation. At that time it was felt that the most sensitive test was the search for the neutron EDM mentioned above [Smith 1951]. As we shall see shortly, this conclusion was not justified because an EDM would violate time-reversal symmetry as well as parity. They (Lee and Yang) suggested experiments to test for parity violation, most notably the measurement of the angular distribution of β rays from a polarized nucleus. If parity were not conserved, there could be electron emission of the form $A = I \cdot p_e$, where I is the nuclear spin and p_e is the electron momentum.

Landau [1957] commented on the unsatisfactory nature of a theory which requires space to be asymmetric with respect to right and left. He suggested that the overall symmetry of space could be preserved in the presence of P violation if the laws of physics were symmetric under the combined operations of charge conjugation and parity performed together (CP symmetry). This was followed rather quickly by the demonstration by Wu et al. [1957] of parity violation in the β -decay of ^{60}Co . Interestingly, the asymmetry was so great that the parity-violating and parity-conserving parts of the interaction needed to explain the results were equal in magnitude; the parity violation in the weak interaction was found to be very large. Later experiments demonstrated that Landau's suggestion was correct and the symmetry obeyed by the weak interaction was indeed CP .

1.1.4. The EDM and time-reversal invariance

In the paper quoted above Landau [1957] also pointed out that one would not see an EDM unless time reversal T is violated in addition to P . The Hamiltonian (1.1) manifests T violation in addition to P violation; under T , $B \rightarrow -B$, $I \rightarrow -I$ and E is unchanged; however, CPT is conserved.

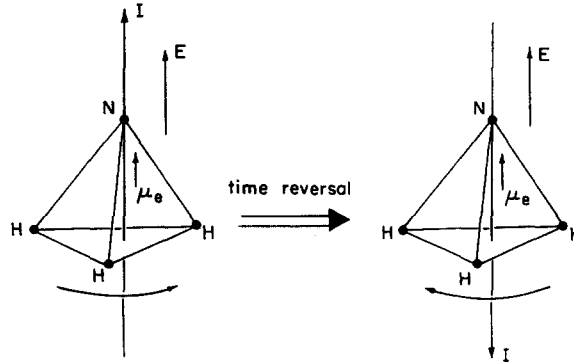


Fig. 1. Normal (left) and time-reversed (right) state of the ammonia molecule; the electric-field strength is great enough so that the Stark effect is linear (the Stark effect energy is much greater than the inversion energy) [Golub and Pendlebury 1972].

Under time reversal, eq. (1.1) is altered; the time-reversed state is different from the original state which implies time reversal is not a symmetry of the Hamiltonian. Why is it then that molecules which have electric-dipole moments are not evidence of time-reversal violation? Figures 1a, b show the normal and time-reversed states of an ammonia molecule. These two states are degenerate and it is this degeneracy which allows the ammonia molecule to have an electric-dipole moment without violating time reversal symmetry. (Actually this degeneracy is removed in ammonia by the inversion splitting, so that the argument only applies in electric fields which are so large that the inversion can be neglected. For smaller electric fields there is a second-order Stark effect.) However, we assumed that the neutron ground state was completely described by the spin projection quantum number m_I and the spin states are nondegenerate. That the neutron ground state is nondegenerate is also supported by the observed fact that neutrons obey the Pauli principle. One can also understand the time-reversal violating character of eq. (1.1) through Kramer's theorem [Messiah 1966] which implies that for a Hamiltonian that depends on an external field which is time-reversal invariant (an electric field, for example) times the angular momentum, the eigenvalues of the system are at least twofold degenerate and the degeneracy is of even order. Since there are only two eigenstates of the neutron, under application of an electric field, these states remain degenerate. The degeneracy is removed by application of a magnetic field.

It had already been recognized that if a local Lagrangian theory is invariant under the proper Lorentz transformation, then CPT (and its permutations) must be a symmetry of the theory (see, e.g., Pauli [1955] and Luders [1957]). After it was recognized that T violation was necessary for the existence of a neutron EDM, Ramsey [1958] argued that time-reversal symmetry was an open question which could only be answered experimentally, i.e., that it was still important to search for the neutron EDM. He again used a possible magnetic charge as a physical model.

1.1.5. Failure of CP invariance

In 1964 Christianson et al. [1964] reported the observation that CP was violated in the decay of the K_0 meson, which implies a T violation as well. Arguments have been given (Casella 1969; Schubert et al. 1970) that the K_0 experiments show T violation directly. This observation of CP violation is the main motivation behind the on-going search for the neutron EDM, and searches for EDMs in other systems, such as atoms [Lamoreaux et al. 1987; Lamoreaux 1989; Hunter 1991].

The origin of the CP violation, discovered in the decay of the K^0 system now 30 years ago, remains an enigma [He et al. 1989; Shabalin 1983]. Historically, experimental upper limits on the

value of a possible neutron EDM (and more recently atomic EDMs) have been used to place severe restrictions on proposed explanations of this decay (see He et al. [1989] and Ellis [1989] for reviews of the theory).

The source of this CP violation remains unknown and experimental upper limits on the value of a possible neutron EDM have been used to place severe restrictions on proposed explanations of this decay. He et al. [1989], Ellis [1989], Barr and Marciano [1989] and Barr [1993] present recent reviews of the theoretical situation while Ramsey [1982, 1978], Golub and Pendlebury [1972] list some earlier reviews. For an example of how the neutron EDM can be estimated from the experimentally observed CP violation in the K^0 system see He et al. [1988].

If the observed baryon-antibaryon constitution of the universe is due to the known CP violation (along with a baryon nonconservation) one can expect a neutron EDM [Ellis et al. 1981]

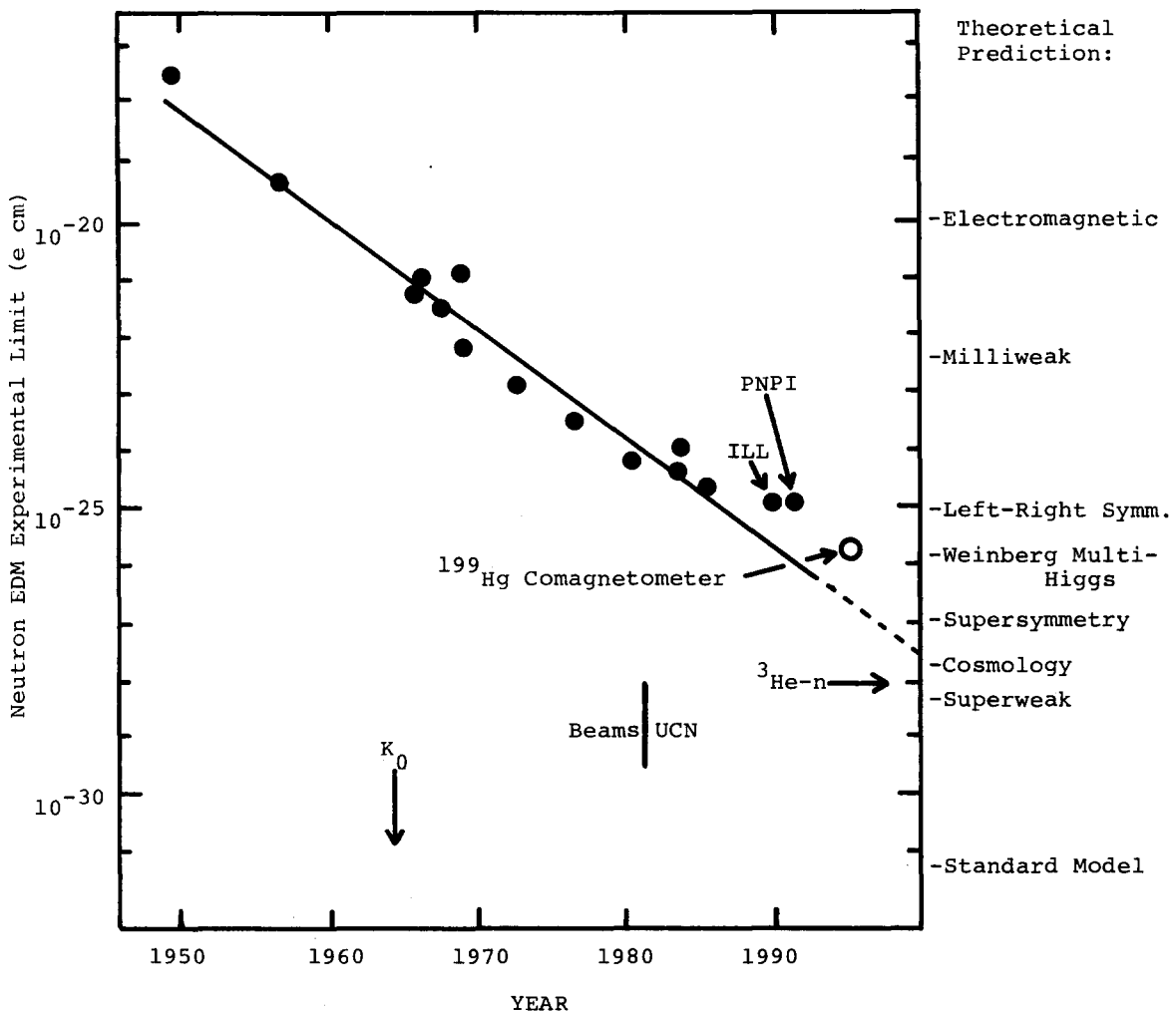


Fig. 2. The history of the experimental limit for the neutron EDM, along with some theoretical predictions. Since the observation of CP violation in K_0 decay (1964) the experimental limit for the EDM has been reducing at a constant rate. The first UCN EDM experimental results were reported in 1981-1982. The most recent limits, from the Petersburg Nuclear Physics Institute and from the Institut Laue-Langevin, are at the level of $10^{-25} e\text{ cm}$. For comparison, the sensitivity expected in the ^{199}Hg comagnetometer experiment is shown, along with that expected in our proposed $^3\text{He-n}$ comparison technique.

$6 \times 10^{-28} < d_n < 2 \times 10^{-25} \text{ cm}$ (cosmology), while the “standard model” leads one to expect an (unobservable) value of [Barr and Marciano 1989; Barr 1993] $10^{-33} < d_n < 10^{-31} \text{ cm}$.

In fig. 2 we show how the experimental precision of the search for a neutron EDM has improved over the years. The most recent experimental values for the neutron EDM are those of Altarev et al. [1992], $d_n = (2.6 \pm 4.0 \pm 1.6) \times 10^{-26} e \text{ cm}$, which they interpret as an upper limit of $|d_n| < 11 \times 10^{-26} e \text{ cm}$, and Smith et al. [1990] (see also Pendlebury [1992]) $d_n = -(3 \pm 5) \times 10^{-26} e \text{ cm}$, which implies $|d_n| < 12 \times 10^{-26} e \text{ cm}$. Both of these experiments made use of bottled UCN.

It is fair to say that the neutron EDM has ruled out more theories (put forward to explain K_0 decay) than any experiment in the history of physics. For example, in Ramsey [1982], roughly 24 out of 35 theoretical estimates are incompatible with the experimental results, while about 16 out of the 17 listed in Golub and Pendlebury [1972] are incompatible. At present, there are 5 or 6 tenable theories [Ellis 1989; He et al. 1989]; continued improvement in the neutron EDM limit will be crucial in determining which of these are correct.

In a recent talk, Weinberg [1992] gave the following review of the current situation: “... endemic in supersymmetry theories are CP violations that go beyond the [standard model], and for this reason it may be that the next exciting thing to come along will be the discovery of a neutron or electron electric-dipole moment. These electric-dipole moments were just briefly mentioned at this conference, but they seem to me to offer one of the most exciting possibilities for progress in particle physics. Experiments here, as in solar neutrino physics move very slowly, but I should mention that there has been a lot of progress lately in calculating the electric-dipole moment of atoms in various models, with results that are encouraging for future experiments.”

2. Current experimental technique

2.1. Ultracold neutrons (UCN)

It was Fermi who first realized that the coherent scattering of slow neutrons would result in an index of refraction, or effective interaction potential V for slow neutrons travelling through matter, and that this potential would be positive (index of refraction $n < 1$) for most materials. This effective potential is crucial for many of the effects grouped together under the topic of neutron optics. Sears [1989] provides a comprehensive discussion of this field.

Fermi also realized that the result of this was that those neutrons (with energy E) incident on a surface at a glancing angle θ which satisfied

$$E \sin^2 \theta \leq V, \quad \sin \theta \leq \sin \theta_c = (V/E)^{1/2}, \quad (2.1)$$

would be totally reflected just as light can be totally reflected on approaching a glass–air boundary from the glass side. Fermi and Zinn [1946] and Fermi and Marshall [1947] performed the first experimental demonstration of this effect. Total reflection of neutrons has provided the basis for the highly successful technique of neutron guide tubes, in which neutrons whose angles satisfy (2.1) can be transported large distances through guides whose surfaces are smooth enough so that nonspecular reflections (reflections for which the angle of incidence is not equal to the angle of reflection) are negligible, as first suggested by Maier, Leibnitz and Springer [1963]. The neutron-guide technique has virtually transformed slow neutron scattering from a rather esoteric technique to one of much wider applications.

The observation of the total reflection of neutrons led to the speculation that if neutrons with energies

$$E \lesssim V \tag{2.2}$$

could be obtained – this is not obvious as typical materials have $V \sim 10^{-7}$ eV while thermal neutrons have energies of 2.5×10^{-2} eV – they would undergo total reflection at any angle of incidence and hence could be stored in closed vessels. We refer to such neutrons as ultracold neutrons (UCN). Golub et al. [1991], Ignatovich [1990] and Steyerl [1977] have presented reviews of UCN research. While many workers in the field of neutron physics attribute the idea of neutron storage to Fermi, the first person to take the idea seriously enough to put it into print was Zeldovich [1959].

He pointed out that although the lifetime of a neutron in, e.g., graphite is only 10^{-2} s (independent of velocity), because of the small penetration depth of a UCN during total reflection ($\sim 10^2 \text{ \AA} = 10^{-6}$ cm) the fraction of the time that stored UCN would actually spend in contact with the walls is quite small ($\sim 10^{-7}$) and so one could expect an absorption time of $\sim 10^5$ s for stored UCN. This is in good agreement with more detailed calculations. Zeldovich also estimated that a thermal flux of $10^{12} \text{ n cm}^{-2} \text{ s}^{-1}$ cooled to 3 K in liquid helium would produce a UCN density of 50 cm^{-3} . It is interesting to note that such densities have now been achieved at the Institut Laue–Langevin, Grenoble using a reactor with a thermal flux of $10^{15} \text{ n cm}^{-2} \text{ s}^{-1}$ cooled to 20 K in a deuterium filled cold source. In 1968, Shapiro published a review article on the electric-dipole moment of elementary particles. In this article he pointed out the advantages of UCN for the search for a neutron EDM, especially the greatly increased observation time and the reduction of the $\mathbf{v} \times \mathbf{E}$ effect (a magnetic field, produced in the frame of the moving neutron by the applied electric field, interacting with the neutron's magnetic moment and mimicking an EDM, as first suggested by Sandars and Lipworth [1964]). See also Golub and Pendlebury [1972] for a more detailed discussion of this point.

Given the fact that the energy V in (2.2) is some 10^5 times smaller than the thermal energy of neutrons in the reactor moderator, and the Maxwellian energy spectrum for neutron flux is proportional to E for low energies, it is remarkable that two groups, independently, had the courage to invest the time and effort to construct the necessary installations on the chance that neutrons so far from the peak of the Maxwell distribution did indeed exist inside the reactor, and that they could be extracted without crippling losses of intensity. That both groups were successful almost simultaneously is one of those coincidences which seem to be so common in the history of physics.

The Dubna group under F.L. Shapiro [Luschikov et al. 1968, 1969] extracted UCN from a very low-power pulsed reactor by means of a curved horizontal channel, 9.4 cm in diameter, 10.5 m long. Counting rates of 0.8 counts/ 10^2 s (background ~ 0.4 counts/ 10^2 s) were obtained. Working at Munich, Steyerl [1969] obtained UCN by vertical extraction from a steady-state reactor. The beam was pulsed by a rotating chopper constructed out of 13 boron silicate glass plates located deep within the reactor swimming pool 2 m above the core, allowing time-of-flight measurements of the neutron spectra. The counting rate showed a steep drop below 10 m/s, probably due to absorption in the aluminium windows, reflection losses and the limited acceptance angle of the detector. However total cross sections were measured for neutron velocities down to 7 m/s for gold and 5 m/s for aluminium.

It is noteworthy that both these initial attempts were made at relatively low-intensity sources, an average thermal flux of $1.6 \times 10^{10} \text{ n cm}^{-2} \text{ s}^{-1}$ in the Dubna experiment and $10^{13} \text{ n cm}^{-2} \text{ s}^{-1}$ in

the Munich experiment, thus demonstrating the ability to carry out really new and important innovations at weak sources.

2.2. Neutron EDM measurements with stored UCN

The neutron EDM is measured by comparing the neutron Larmor frequency (measured, for example, by use of Ramsey's method of separated oscillatory fields [Ramsey 1956]) for parallel and for antiparallel magnetic and electric fields. It follows from eqn. (1.1) that the shift in Larmor frequency between the two field configurations is $\delta\omega_0 = -4d_n E/\hbar$; the minus sign is necessary because $\mu_n < 0$.

Following the first experiments on UCN production Okun [1969] called attention to Shapiro's [1968] point that UCN offered a promising method for improving the sensitivity of the search for a neutron EDM, emphasizing the potential improvement in observation times— 10^3 s for UCN compared to 10^{-2} s in a typical beam experiment.

Lushchikov et al. [1969] also suggested that UCN could be used to search for a neutron EDM. It was immediately recognized that a storage experiment could give orders-of-magnitude higher sensitivity than a beam experiment due to a longer interaction time, 10^2 s as opposed to 10^{-2} s, and that systematic effects due to nonparallel E and B fields would be greatly suppressed. Golub and Pendlebury [1972] discuss fundamental limits to sensitivity for a variety of neutron EDM experiments; use of bottled UCN is the clear winner. They further suggest, "if no effort were spared a limit for the dipole length of 5×10^{-27} e cm might ultimately be reached." The present experimental limits are not too far from this and this level is expected to be reached in the next round of measurements. As we shall see later a factor of 1000 further improvement in sensitivity seems possible.

An important advantage to the use of bottled UCN over beam experiments is the elimination of the systematic effect due to the magnetic field generated by $\mathbf{v} \times \mathbf{E}$; if \mathbf{E} and \mathbf{B} are not exactly parallel,

$$\delta B = (v/c)E \sin \theta_{EB} + \sqrt{B^2 + [(v/c)E]^2}, \quad (2.3)$$

where it is assumed that the velocity, \mathbf{v} , is approximately perpendicular to \mathbf{E} . \mathbf{E} and \mathbf{B} are roughly parallel and $\theta_{EB} \approx 0$ is the angle between the magnetic and electric fields [Sandars and Lipworth 1964]. In the case $\theta_{EB} \neq 0$, there is a change in magnetic field associated with the application of the electric field which generates a shift in Larmor frequency indistinguishable from an EDM shift. In addition, even if the fields are parallel, there is a shift in magnitude proportional to E^2 ; thus it is required that the magnitude of the electric field be reversed exactly in any case, something which can be difficult in the presence of dielectrics. Since UCN stored in a bottle have an average velocity of approximately zero, $\mathbf{v} \times \mathbf{E}$ effects are substantially reduced.

We will now derive the fundamental limits to a general class of bottled UCN experiments, which include the neutron electric-dipole moment search, where a shift in energy between the two spin states (a shift in Larmor precession frequency ν) due to the application of an external field is measured using magnetic-resonance techniques. The magnetic resonance linewidth, which determines the accuracy for which a shift can be measured, is given by

$$\Delta\nu \propto 1/T, \quad (2.4)$$

where T is the time that the neutron spin was in a coherent superposition (precessing about the field). This is a restatement of the uncertainty principle, that $\delta E \delta T \geq 1$ (energy measured in Hz). Again, there is a finite neutron survival time τ with the total number at time t given by

$$N(t) = N_0 e^{-t/\tau} . \quad (2.5)$$

The fluctuations in ν between measurements due to counting statistics can be readily determined (assuming that the total storage time is equal to T , the coherence time),

$$\delta \nu \propto (1/\alpha T) N_0^{-1/2} e^{T/2\tau} . \quad (2.6)$$

where α represents the polarization efficiency. Assuming again that we do many (n), experiments over a time $t \gg T$, we find, using $n = t/T$, that

$$\sigma(\nu) \propto N_0^{-1/2} \alpha^{-1} e^{T/2\tau} / \sqrt{tT} . \quad (2.7)$$

This has a minimum when $T = \tau$. Thus, it is evident that we want a long survival time, α nearly one, and N_0 to be large.

As was already mentioned, use of Ramsey's method of separated oscillatory fields is a convenient way to measure the magnetic-resonance frequency [Ramsey 1956]. In this method, we start with the spin along a static magnetic field. An oscillating magnetic field nearly at the Larmor frequency and perpendicular to the static field is turned on for a time τ' such that the spin (as viewed in the rotating frame) precesses through 90° , that is, a $\pi/2$ pulse; the magnitude of the field $2b$ and τ' satisfy the relation $\gamma b \tau' = \pi/2$, where γ is the magnetic moment. After the oscillating (or RF) field is turned off, the spin precesses about the static field for a time $T \gg \tau'$, at which time a second pulse is applied; note that the oscillator has been running in the background and has complete phase coherence as defined by the first pulse. However, if the Larmor frequency and RF frequency are not exactly equal, a phase difference builds up $\phi \approx (\omega - \omega_0)T$, where ω is the RF frequency and $\omega_0 = \gamma B$ is the Larmor frequency. Thus, in the rotating frame, the spin is not at right angles to the RF field and, after a second $\pi/2$ pulse, the spin will end up at an angle ϕ to the static field. The final polarization is given by $-P_0 \cos \phi$. As the RF is tuned off of resonance, the initial spin-flip probability is reduced, thus the oscillations die away as shown in fig. 3.

An important advantage of bottled UCN over beam experiments is that the timing conditions are the same for all neutrons. In a beam, faster neutrons spend less time, slower ones more time, hence the Ramsey fringes get washed out. However, in the neutron bottle, if the RF field is sufficiently homogeneous and if τ' is longer than the mean collision time so that the RF field is sufficiently averaged, all the neutrons see the same pulse length, and the same time between pulses, thus the beautiful pattern shown in fig. 3. Since the time between pulses T , is the same for all neutrons, all the neutrons have $\cos \phi = 0$ at the same frequency and all the maxima in fig. 3 are the same height (transition probability = 0).

When separated oscillatory fields are used, the determination of the effective linewidth is not so obvious. If we use eq. V.37 given by Ramsey [1956] in the limit $b \gg \Delta\omega$ where $\Delta\omega = \omega_0 - \omega_{\text{rf}}$ and b is the rf field strength, and if $\pi/2$ pulses are used (that is, the pulse length τ' and the rf field strength satisfy the condition $\tau' \gamma b/2 = \pi/4$), we find that the probability to flip the neutron spin is

$$P \approx -\cos \Delta\omega T , \quad (2.8)$$

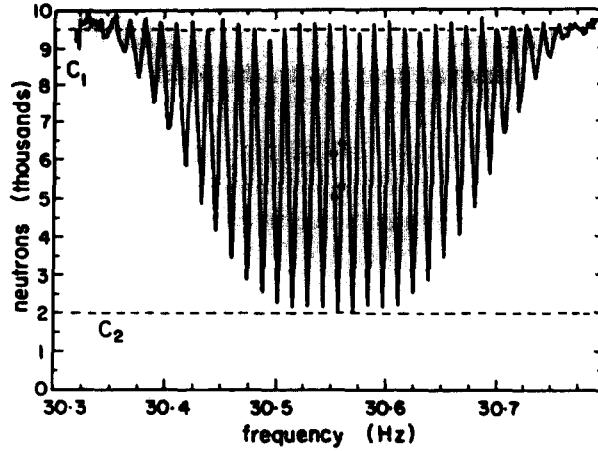


Fig. 3. A neutron magnetic-resonance curve using the Institut Laue–Langevin EDM apparatus which employs Ramsey’s method of separated oscillatory fields. The polarized UCN were stored for a total of 80 s; the time between the 4 s $\pi/2$ pulses was 68 s, giving a linewidth of 7 mHz for the central fringe. Under normal operation of the apparatus, data is taken sequentially between the four points shown; this provides a continuous calibration of the apparatus [Smith et al. 1990].

where $T \gg \tau'$ is the time between pulses, which is the same result as our qualitative argument above. If we use the same polarizer for both initial polarization and for analysis after the two pulses, and take into account the polarizer inefficiency, we find that the number of neutrons which get through the polarizer is

$$N(\Delta\omega) = N_0(1 - \alpha \cos \Delta\omega T)/2, \quad \alpha = (C_1 - C_2)/(C_1 + C_2), \quad C_1 = N_0, \quad (2.9)$$

where α is the visibility as in fig. 3.

Since we will be looking for a small change in frequency with application of the electric field, we want to sit on the side of the resonance where the sensitivity is highest, that is, where the slope in the number of counts versus $\Delta\omega$ is highest, and look for a change in counts with application of the electric field,

$$\partial N(\Delta\omega)/\partial\Delta\omega = N_0 \frac{1}{2} \alpha T \sin \Delta\omega T. \quad (2.10)$$

We need to minimize

$$\sigma(\Delta\omega) = [\partial\Delta\omega/\partial N(\Delta\omega)] \sqrt{N_0}, \quad (2.11)$$

since we count a total of N_0 neutrons for both spin states. This has a minimum at $\Delta\omega T = \pi/2$ where we find the frequency noise due to counting statistics

$$\sigma(\Delta\omega) = 2/\alpha T \sqrt{N_0}, \quad (2.12)$$

where N_0 is the number of counts for both spin states. Using our hamiltonian, eq. (1.1), and $\delta\omega = -2d_n E/\hbar$, leads to

$$\sigma(d_n) = 1/\alpha ET \sqrt{N(\Delta\omega)}. \quad (2.13)$$

2.3. Recent EDM experiments using UCN

2.3.1. Bottled UCN EDM experiment at the Institut Laue–Langevin

Figure 4 is a schematic of the experimental apparatus which is described more fully in Miranda [1987] and Pendlebury et al. [1984]. The apparatus was initially used on the old ILL PN5 UCN source and produced the result $0.3 \pm 4.8 \times 10^{-25} e \text{ cm}$ [Pendlebury et al. 1984]. In 1986, the experiment was moved to the ILL neutron turbine [Steyerl et al. 1986], where the UCN flux is two orders of magnitude higher; the UCN density at the turbine output is 90 cm^{-3} . The new result of this experiment is $-(3 \pm 5) \times 10^{-26} e \text{ cm}$ [Smith et al. 1990]. A description of the experiment follows.

The UCN are transported from the turbine to the experiment through a stainless steel guide. At the apparatus, the UCN are polarized by transmission through a magnetically saturated $1 \mu\text{m}$ thick iron–cobalt foil. The neutron bottle, consisting of two beryllium electrodes 0.25 m in diameter separated by a 0.1 m long cylindrical beryllium oxide tube (0.01 m thick wall) which serves as an insulator, has a net critical velocity 6.9 m/s . The BeO tube rests in grooves, about twice the tube thickness deep, in the Be plates. This arrangement gives better high-voltage stability. The ideas and technology behind the BeO–Be bottle are described by Golub [1986]. Neutrons enter the bottle through a hole, which can be sealed with a beryllium door, in the grounded electrode.

The bottle is inside a five-layer Permalloy shield (shielding factor of 10^5) [Sumner et al. 1987] with the bottle axis perpendicular to the cylinder axis of the shield, the orientation being such that the magnetic shielding is maximum. A $1 \mu\text{T}$ magnetic field B , parallel to the axis of the bottle, is produced by a cylindrical coil with a constant number of turns per unit distance perpendicular to the axis of the shield (cosine distribution), to produce a uniform field inside the magnetic shield.

The magnetic field between the polarizer and the storage bottle was carefully tailored so that the adiabatic condition, $\omega_L = \gamma B \gg |dB/dt|/B$, where γ is the gyromagnetic ratio, is satisfied, and so that $B \neq 0$ everywhere; thus there is a gradual change from the approximately one kilogauss polarizer field to shield, and through the shield to the bottle field of 10 mG ; thus no loss of polarization occurs.

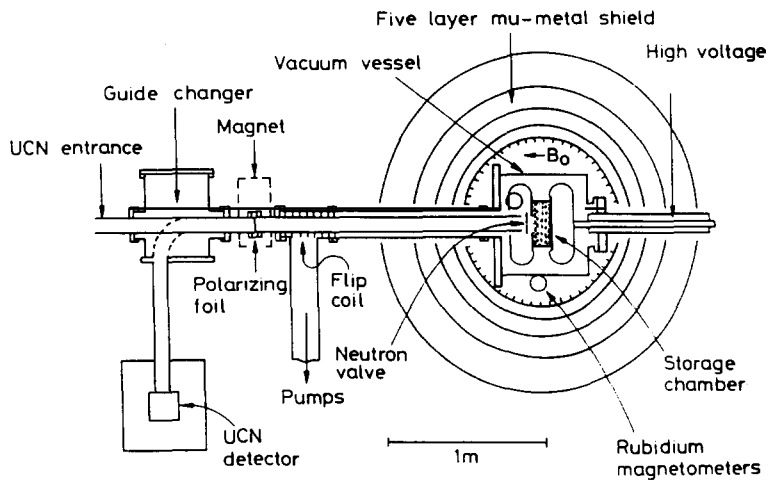


Fig. 4. The neutron EDM measurement apparatus used at the Institut Laue–Langevin. The UCN are stored for a total of 80 s ; the static magnetic field is 10 mG and the applied electric field about 10 kV/cm [Smith et al. 1990].

The experiment is operated as follows. The five-liter storage volume is filled for 10 s (three filling time constants), after which the door is closed. Immediately after filling, the density of polarized UCN is about 10 cm^{-3} . After waiting 6 s to allow the neutron velocities to become isotropic within the bottle, the first pulse of a Ramsey separated (in time) oscillatory-field magnetic-resonance sequence [Ramsey 1956] is applied for 4 s. This turns the neutron spins perpendicular to the magnetic field. The neutrons are allowed to precess for 70 s (the neutron storage lifetime) after which a second 4 s Ramsey pulse is applied. The neutron valve is opened and those neutrons in the appropriate spin state pass through the polarizing foil which now serves as an analyzer, are diverted to a detector, and are counted for 10 s. The spin-flip coil, which consists of about 5 turns/cm wound on a NiCu coated glass guide (so that the 3 kHz rf field can penetrate) 20 cm long, is then turned on and adiabatically reverses the spin, thereby permitting the remaining neutrons to pass through the polarizing foil and be counted, also for 10 s. The two counting periods give approximately 12 000 and 8000 neutrons. Including filling and emptying, each measurement cycle takes 124 s.

An electric field, E , with magnitude up to 1.6 MV m^{-1} , follows a 32-measurement cycle (about one hour) sequence: eight cycles applied parallel to B , four cycles off, eight cycles antiparallel, and four cycles off, with two cycles taken to change each state (the magnitude of E is constant over each approximately three-day set of measurements). The direction of E is reversed by simply changing the polarity of the voltage applied to the upper plate. The neutron bottle is maintained under vacuum (10^{-6} torr) or with 10^{-4} torr of nitrogen or helium to help quench sparking; it was found that helium works much better. Leakage currents across the bottle are monitored and are kept below 30 nA by operating at an appropriate voltage. For most of the data presented here, the leakage current was less than 5 nA.

Over the course of a reactor cycle (about six weeks), the neutron-storage and high-voltage properties of the bottle gradually deteriorate. This is probably due, in part, to hydrogen contaminating the surface [Lanford and Golub 1977]. The background system vacuum is rather poor, of order 10^{-6} torr. Running a discharge of Ar and D_2 in situ (about 150 V, 50 Hz for 10 min at 1–5 Torr) restores the storage time [Mampe et al. 1981] and low-leakage currents. Such discharge cleaning is repeated approximately once every reactor cycle. There is some evidence that the presence of high voltage accelerates the degradation.

The magnetic field within the shield is monitored using three optically pumped rubidium magnetometers placed around the neutron bottle [Pendlebury et al. 1984] at a maximum distance of 40 cm from the bottle. The field at each magnetometer is averaged over the neutron-storage time. In addition, there is a flux gate magnetometer placed between the outer two layers of the shield to check for possible externally generated systematic signals.

Between measurements, the frequency of the rf field for Ramsey pulses is changed so that there can be a continuous calibration of the apparatus; the frequency is varied sequentially through four points around the central fringe of the resonance pattern (see fig. 3). The two points on each side of the resonance center are separated by one tenth of a linewidth. The four points are used to determine both the neutron-spin polarization and the resonance frequency. To determine the neutron resonance frequency, ν_n , a first pass is made through the data to extract the visibility of the resonance curve, $\alpha = (C_1 - C_2)/(C_1 + C_2)$, which is typically 0.64 (see fig. 3). A second pass uses α and a combination of the counts for the two neutron-spin states to yield a single resonance frequency ν_n for each measurement cycle, as implied by eq. (2.9). An important advantage of this technique is that it suppresses nonstatistical fluctuations in the neutron flux (due to reactor-power fluctuations, for example), since one works with the ratio of spin-up to spin-down counts. Over the course of the measurements, the frequency is changed so that the resonance is tracked as the magnetic field drifts.

A run lasts about three days and has about 1000 measurements of the resonance frequency. The electric field is reversed about every ten measurements as described above.

An EDM would appear simply as a shift in resonance frequency with application of an electric field. The problem is to extract the EDM frequency shift from other systematic effects due to sparks, leakage currents, or externally generated fields associated with switching the high voltage.

A number of techniques have been used to extract the neutron frequency shifts which change sign with the applied electric-field direction, $\Delta\nu_n = \frac{1}{2}[\nu_n(E) - \nu_n(-E)]$. Generally, a drifting background is removed by fitting terms linear and quadratic in time for the individual measurement sets. Cycles around obvious discrete jumps in the magnetic field are discarded. Similar analyses are performed for the three magnetometers yielding $\Delta\nu_{m1}$, $\Delta\nu_{m2}$, and $\Delta\nu_{m3}$. Frequency shifts quadratic in E (voltage-on–voltage-off effects) and shifts between the zero electric-field groups (due for example to the shields being magnetized by leakage currents or sparks) are also extracted. To help identify systematic effects, the direction of the fixed magnetic field is reversed every few weeks; a true EDM frequency would have its sign reversed by this. In addition, the high voltage was varied between measurement sets; a true EDM would scale with the electric-field strength.

The magnetometer readings have been used to correct for systematic errors in two independent ways. The conclusion is that the best result for the neutron EDM comes from the average of the results of the two different analyses, with the larger of the two error bars,

$$d_n = (-3.3 \pm 4.3) \times 10^{-26} e \text{ cm}, \quad |d_n| < 12 \times 10^{-26} e \text{ cm } 90\% \text{ C.L.}$$

The contribution to the above error from neutron counting statistics, using eq. (2.13), is $1.9 \times 10^{-26} e \text{ cm}$.

The present experiment is limited by how well the magnetic field within the neutron bottle is monitored by the spatially separated rubidium magnetometers. In section 2.3.3 we will describe a new experiment which is being built from the components of this experiment, incorporating a comagnetometer (a polarized atomic species within the neutron-storage volume); this should give an improvement of a net factor of ten.

2.3.2. Bottled UCN EDM experiment at the VVR-M reactor, Leningrad

Altarev et al. [1992] have recently reported the result $d_n = (2.6 \pm 4.0 \pm 1.6) \times 10^{-26} e \text{ cm}$, which they interpret as an upper limit of $d_n < 1.1 \times 10^{-25} e \text{ cm}$. This should be compared with their earlier result [Altarev et al. 1986] $d_n = -14 \pm 6 \times 10^{-26} e \text{ cm}$. The major improvements for this experiment were in the UCN source and an increased neutron-storage time.

A schematic of the experimental apparatus is shown in fig. 5. In many ways the apparatus is similar to that of the ILL experiment, however, there are important differences. As can be seen in fig. 5, there are two neutron-storage chambers with oppositely directed electric fields (relative to the magnetic field) in each chamber. The high voltage is applied to the plate separating the two chambers while the outer plates are held at ground potential. They typically run at 15 kV/cm, somewhat higher than the average of the ILL experiment.

Using two bottles with oppositely directed electric fields essentially doubles the sensitivity to a neutron EDM while reducing background magnetic-field noise; an EDM-generated shift will be of opposite sign for the two chambers. In addition, since the two chambers are located quite close spatially, one would expect high discrimination from background magnetic-field changes since the EDM shift is given by the difference in the resonance frequency between the chambers as a function of electric-field direction; this difference is sensitive only to changes in spatial gradients of the magnetic field. Such gradients could be due to locally generated fields such as leakage currents

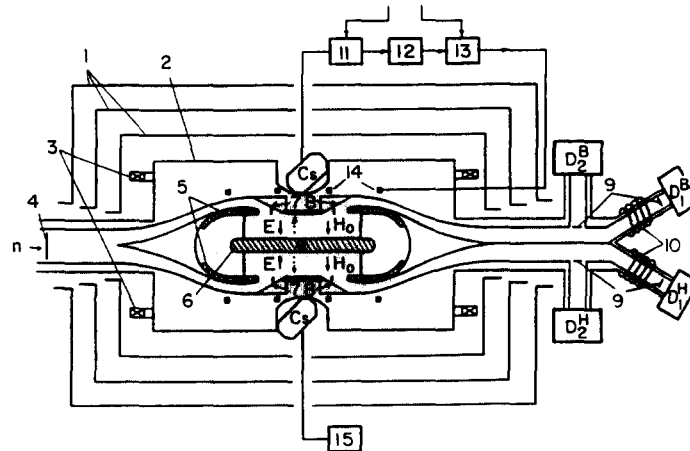


Fig. 5. The neutron EDM measurement apparatus used at the Petersburg Nuclear Physics Institute, Gatchina, Russia. 1. magnetic shields, 2. vacuum chamber, 3. Helmholtz coils for producing the static magnetic field, 4. UCN polarizer, 5. ground electrode, 6. high-voltage electrode, 7. entrance shutter, 8. exit shutter, 9. spin analyzers, 10. spin flipper, 11. cesium magnetometers, 12. frequency divider, 13. control for oscillating-field pulses, 14. coils for producing oscillating field, 15. cesium magnetometer. D labels the UCN detectors with B and H specifying upper and lower chambers, 1 and 2 specifies the two polarizations. Two quartz insulating rings together with the three electrodes comprise the two storage volumes of 20l each [Altarev et al. 1986].

within the bottle. However, even for local fields, the close placement of the chambers should give a fairly good cancellation of the net magnetic-field change.

The position of the resonance is stabilized by synthesizing the radiofrequency pulses for the neutrons from the output of two cesium magnetic Zeeman atomic oscillators (located near the storage chambers). (The ratio of neutron resonance frequency to cesium is about 120.) This was necessary in part because the three-layer Permalloy shield did not provide adequate stability and shielding. The stabilization improved the effective shielding by a factor of about 15.

The chamber walls are quartz rings onto which films of BeO and Be_3N_2 have been deposited. Leakage currents average 30 nA at the approximately 15 kV/cm used. There is a system of shutters to the entrance and exit guides through which the chambers can be filled and emptied. A system of four detectors, each with its own polarizer and two with adiabatic spin flippers allow counting the spin-up and spin-down neutrons for each chamber simultaneously, as opposed to the ILL experiment where the spin-up and spin-down are counted in sequence.

The experiment originally operated in a “flow-through” mode; that is, the neutron shutters were kept continually open and neutrons were continuously counted; a shift between spin-up and spin-down counting rate as a function of electric-field direction would be an indication of an EDM. However the majority of the data leading to the published results was obtained using a pulsed technique similar to that used in the ILL experiment, making full use of the chamber lifetime of 50 s as implied by eqs. (2.7) and (2.13). The increase in sensitivity gained here along with the improved source of UCN results in a daily statistical uncertainty of about $2.5 \times 10^{-25} e \text{ cm}$, comparable to the ILL experiment.

The data reported in Altarev et al. [1986] seemed to have some systematic contamination. In Altarev et al. [1992] the authors attributed a large part of the discrepancy between their newest result and that of 1986 (see above) to the result of a single run. After discarding this run the 1986 result is more or less in agreement with the later one.

2.3.3. UCN EDM experiment with a ^{199}Hg comagnetometer

Since the ILL experiment described in section 2.3.1 was no longer limited by counting statistics but by systematics, it was decided to rebuild the apparatus and include a comagnetometer, that is, a polarized atomic species within the same storage volume as the neutrons, and thus provide a nearly exact spatial and temporal average of the magnetic field as seen by the neutrons over the storage period. The use of polarized ^3He had already been considered [Ramsey 1984], but the extreme difficulty in the detection of the ^3He polarization makes its use impractical.

The use of ^{199}Hg has been suggested [Lamoreaux 1986] and a magnetometer suitable for the EDM experiment has been constructed and tested [Pendlebury 1992]. The advantage here is that ^{199}Hg can be readily directly optically pumped and its polarization optically detected with 254 nm resonance radiation [Lamoreaux 1989]. Since ^{199}Hg is a $^1\text{S}_0$ atom, its ground-state polarization is specified by the nuclear angular momentum, which is $1/2$ for ^{199}Hg .

An important feature of a spin- $1/2$ system is that its Larmor frequency cannot be affected by electric fields other than through an EDM. This is a statement of Kramer's theorem, already mentioned above, that the energy levels of a T -even hamiltonian are doubly degenerate [Messiah 1966]. Since there are only two levels which describe the ground state, these levels are degenerate and there is no observable effect. This is to be compared to higher-spin species which were earlier considered, such as alkali atoms (cesium and rubidium). In these cases, the total spin is greater than 1 and the atoms have a large electric polarizability; the ground-state Zeeman levels split proportional to E^2 . Such shifts would make exact reversal of the electric field imperative, an experimental difficulty in the presence of dielectrics.

Furthermore, it is necessary that the atomic species does not have an EDM of its own which could possibly mask a neutron EDM; in the case of ^{199}Hg , experimental limits have already been set at the level of sensitivity needed [Lamoreaux et al. 1987; Lamoreaux 1989]. In these experiments, ground-state spin-polarization lifetimes in excess of 100 s were routinely achieved in cells of about 5 cm^3 volume, even in the presence of electric fields up to 15 kV/cm . However, these cells included 250 torr of nitrogen to improve the high-voltage stability.

An unfortunate disadvantage of ^{199}Hg is that the walls of the container must be specially prepared to have long spin-relaxation times. In all previous experiments, hydrocarbon waxes were used; these of course would be unusable with UCN. In addition, the wall coating has to be stable under the application of high voltage in vacuum since a high-pressure background gas cannot be used with the UCN.

A possible wall coating material, deuterated polystyrene (DPS), has been developed [Lamoreaux 1988] and is presently in use [Pendlebury 1992]. Although the Hg spin polarization characteristics are not as good as the hydrocarbon waxes, (10 s/cm mean free path versus 100 s/cm mean free path), it should give a lifetime of about 100 s in the much larger neutron bottle. In addition, thin films of DPS seem to be stable under electric fields in vacuum. The vacuum stability is a bit puzzling as every other thin-film (suitable for use with UCN) material tested would break down at relatively low electric fields. These materials included fomblin and teflon where electric fields of about 2 kV/cm would cause breakdown. It has long been known that polystyrene can be formed from an electrical discharge in styrene vapor; perhaps there is some complicated dynamical chemistry which leads to the high-voltage stability. In addition, it has been shown that for a material to have high-vacuum-voltage stability, its vapor pressure must increase slowly with temperature [Trump and Van de Graaff 1947]. The vapor pressure of fomblin certainly rises rapidly with temperature, hence its usefulness as a diffusion pump fluid. Teflon breaks down readily upon heating; the breakdown temperature of polystyrene seems to be higher than that of teflon.

DPS also has excellent UCN storage properties. Preliminary tests show that it is about as good as fomblin and as easy to apply to a surface. The Fermi potential of DPS is about 165 neV, higher than that of fomblin. In addition, thin films of DPS are stable in vacuum even under application of electric fields. It should be pointed out here that teflon has good polarized Hg storage properties and the surface can be adequately prepared for arbitrarily large bottles; its only drawbacks are its instability in high voltage, although this problem might be solved, and its somewhat lower Fermi potential.

Spin relaxation times for ^{199}Hg of 15 s in a 22 ℓ bottle coated with DPS have been reported [Pendlebury 1992]. It has since been discovered that atomic hydrogen on the surface severely impairs the lifetime (for both teflon and DPS) and that a weak discharge in approximately 0.1–1 Torr oxygen cleans the surface and gives a good lifetime of 70–80 s, in good agreement with the expected 100 s, which remains stable under clean vacuum conditions [Lamoreaux 1992].

A schematic of the experimental apparatus is shown in fig. 6. To increase the sensitivity through storage time and neutron counts, and to account for the loss of neutrons due to the lower Fermi potential of DPS over Be–BeO, a larger (about ten times) volume storage bottle has been constructed. Since there is a considerable shift in the center of mass between the UCN gas and atomic gas in the gravitational field (due to the difference in temperature) [Ramsey 1984], the experiment is designed so that the shorter axis of the bottle is vertical, thus minimizing the displacement. It is necessary to have a gas-tight window which can withstand atmospheric pressure. It has been decided that this will be the polarizer; the polarizer is constructed by evaporating iron onto aluminum. To account for the fairly high Fermi potential of the aluminum,

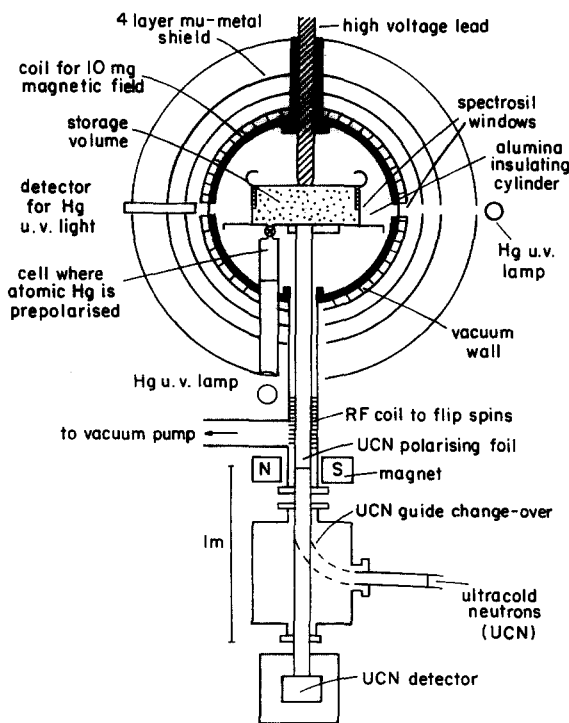


Fig. 6. The modified ILL EDM apparatus which now includes a ^{199}Hg comagnetometer. The chosen height of the apparatus maximizes the UCN density after a 120 s storage period. The Hg spin orientation is detected by a beam of circularly polarized resonance radiation propagating across the storage volume [Pendlebury 1992].

after passing through the foil the UCN will rise about one meter. Tests have been conducted to determine the optimum combination of heights to maximize the number of UCN left in a test bottle after a 100s storage period.

The neutron-storage bottle is an aluminum oxide cylindrical spacer about 60 cm in diameter and 20 cm high separating the aluminum plates. The entire inner surface has been coated with DPS. The neutron valve is gas-tight to minimize the loss of the polarized atomic vapor.

Provisions are included for polarizing the atomic vapor. There is an optical pumping cell connected to an isotopically enriched Hg reservoir. The Hg is optically pumped to the appropriate spin state, parallel to the static field, with circularly polarized light from a Hg discharge lamp. After the Hg is polarized, and after the neutron bottle is filled with polarized UCN and the neutron valve closed, the polarized Hg is admitted to the neutron bottle. $\pi/2$ pulses are applied for both the neutrons and Hg (the ^{199}Hg magnetic moment is about one third of the neutron magnetic moment). The free precession of the Hg spin is observed with a beam of circularly polarized resonance light which propagates across the bottle diameter, through quartz windows in the insulating cylinder. The average magnetic field over the storage time can be determined from the free precession signal.

At the end of the storage period, the second neutron pulse is applied, the bottle door opened, and the neutrons are counted as usual. The Hg is pumped away. While the storage was in progress, more Hg had been admitted to the optical pumping cell and polarized; the process is thus ready to be repeated.

An EDM will be evident from a change in the ratio of the magnetic moments between reversals of the electric field. Although the sensitivity of the Hg to the magnetic field is only 1/3 that of the neutron, the high signal-to-noise inherent in the free precession signal is a compensating factor; in fact, preliminary estimates show that determination of the average field should be a factor of 10 higher in sensitivity than the neutron signal and hence contribute very little noise.

3. Superfluid He neutron EDM with ^3He comagnetometer

3.1. Introduction

Golub [1983, 1987] has suggested performing an EDM search directly in the liquid helium of a superthermal source [Golub et al. 1983; Kilvington et al. 1987] using a dilute solution of polarized ^3He as a polarizer and detector since ^3He absorbs neutrons only when the total spin is zero (neutron and ^3He spins antiparallel). The polarization and transport of polarized ^3He is a well-developed technology [Aminoff et al. 1989]. The reaction between ^3He and neutrons should produce ultraviolet scintillation in the liquid helium which should be easily detectable, giving a detection of $^3\text{He-n}$ reactions with nearly 100% efficiency. In addition, liquid He has good dielectric characteristics and it should be possible to establish modest electric fields without breakdown.

Such an experiment would be sensitive to a neutron EDM by looking at the scintillation rate at the end of a double-pulse sequence as a function of electric field. It has been shown, by solving the Schrödinger equation in the presence of a spin-dependent absorption probability, that this technique is slightly less sensitive than the conventional bottle technique; however, this loss of sensitivity is more than made up for by elimination of the extraction losses, transport losses, polarization transmission losses, etc. In fact, extremely high UCN densities might ultimately be achieved by locating the helium as close as possible to the reactor core. In addition, the presence of

liquid helium suggests the use of superconducting shields which might be better than the usual Permalloy.

Unfortunately, the problem of measuring the magnetic field remains and it has been demonstrated that experiments are presently limited by magnetic systematic effects. It might be possible to use SQUID magnetometers to detect the ^3He magnetization, the ^3He could then serve as a magnetometer. However, the sensitivity is at best marginal. Lamoreaux and Golub [1989] have suggested using the ^3He as a direct comagnetometer by using “dressed atom” techniques to make the magnetic moments of the neutron and ^3He equal. In this section we will describe the method using a classical model. In section 4 we give a quantum-mechanical discussion of the dressed spin system while section 5 gives a quantum-mechanical discussion of the evolution of the system under the influence of modulated dressing and feedback from the EDM signal to the dressing parameters. In section 6 we present an analysis of the expected accuracy of the method while section 7 discusses some relevant technical questions.

The main idea is to make use of the production of UCN by the downscattering of 8.9 \AA neutrons in superfluid ^4He . If the ^4He contains a very small concentration of polarized ^3He , the UCN will be polarized due to the strong spin dependence of the ^3He absorption cross section. Since the ^3He will be exposed to the same magnetic field as the UCN, the precession of the ^3He can be used as a comagnetometer, measuring the volume and time average of the magnetic field as seen by the UCN [Golub 1983]. In fact, as we show below, the effects of the static magnetic field can be completely eliminated by the “critical dressing” technique [Golub et al. 1991; Lamoreaux and Golub 1991]. Because of the spin dependence of the ^3He absorption cross section, the UCN absorption rate will depend on the angle between the ^3He and the UCN spins. By detecting the scintillations produced in the ^4He due to the energetic triton and proton released following UCN capture by ^3He , the ^3He can be made to serve as polarization analyzer and UCN detector.

A reasonable goal is to gain a factor of $1-5 \times 10^2$ in EDM sensitivity over that anticipated in the Hg comagnetometer experiment. This could be from a factor of 3–5 increase in electric field which should be allowed by the rather good insulating properties of liquid helium, a factor of 100 in statistics due to a factor 10^4 increase in the total number of UCN (from an increase in UCN density and a larger storage-chamber volume), and an increased storage lifetime, from 80 s in the present experiments to 500 s.

3.2. Production of UCN in superfluid ^4He

Neutrons at (or near) rest in a bath of superfluid ^4He can only absorb a ^4He excitation whose energy and momentum E_c, k_c lie at the intersection of the well known ^4He phonon–roton dispersion curve and the “free-neutron dispersion curve” [Golub et al. 1983],

$$\omega = \hbar q^2 / 2m_n . \quad (3.1)$$

This process is strongly suppressed by the Boltzmann factor, $\exp(-E_c/T)$, where $E_c \approx 11 \text{ K}$. By the same argument only neutrons with energies at (or near) E_c can scatter into the UCN energy region by emission of a single excitation. The UCN produced in this way will remain in the helium until they are lost through one of the possible loss mechanisms (β decay, absorption by ^3He , wall losses, upscattering). The UCN will reach a saturation density

$$\rho_{\text{UCN}} = P\tau , \quad (3.2)$$

where P is the production rate ($\text{cm}^{-3} \text{s}^{-1}$) due to the above-mentioned downscattering, and τ is the storage lifetime due to all loss mechanisms [Kilvington et al. 1987].

As the UCN are produced independently of the direction of the incoming neutrons it is possible to increase P and hence ρ_{UCN} by increasing the solid angle of the incoming neutron beam.

Since the present experiment has a density of 3–4 UCN/ cm^3 , to achieve a 10^4 increase in density requires a production rate of 60 UCN/ $\text{cm}^3 \text{s}$ (assuming a storage lifetime $\tau \sim 500 \text{s}$) which can be compared to the production rate of 2/ $\text{cm}^3 \text{s}$ obtained in the present superthermal source experiments carried out at the end of a neutron guide [Kilvington et al. 1987].

3.3. Polarization of UCN

The fraction of the total neutron absorption by ^3He which takes place from the $J = 0$ state was measured to be [Passell and Schermer 1960]

$$\sigma_{J=0}/\sigma_{\text{tot}} = 1.01 \pm 0.03, \quad (3.3)$$

so that we can assume that there is no absorption for the neutron spin s_n parallel to the ^3He spin s_3 ($J = 1$),

$$\sigma_+ = 0, \quad \sigma_- = 2\sigma_0, \quad \sigma_0 = 5.5 \times 10^3 \text{ b}, \quad (3.4)$$

where σ_0 is the ^3He absorption cross section as usually measured ($v_n = 2200 \text{m/s}$ and both the neutrons and ^3He unpolarized) and \pm indicate the relative directions of the UCN and ^3He spins (+ for parallel). The storage lifetime of the two different spin states is then

$$1/\tau_{\pm} = 1/\tau_{\text{w}\beta} + (1 \mp P_3)(N_3 \sigma_0 v_n), \quad (3.5)$$

where $\tau_{\text{w}\beta}$ is the effect of wall losses and β decay and P_3 , N_3 are the ^3He polarization and number density, while v_n represents the neutron velocity at which σ_0 is measured. Due to the $1/v$ dependence of absorption cross section (note that it is the UCN velocity relative to the center of mass of the ^3He gas which is important here) $\sigma_0 v_n$ is a constant independent of neutron velocity.

Thus the saturation UCN densities for the two spin directions are

$$\rho_{\pm} = \frac{1}{2} P \tau_{\pm}, \quad (3.6)$$

leading to

$$P_{\text{UCN}} = P_3 / (1 + \tau_{\text{He}}/\tau_{\text{w}\beta}) \quad (3.7)$$

for the UCN polarization, where $1/\tau_{\text{He}} = N_3 \sigma_0 v_n$. The absorption rate of UCN by ^3He or the rate of production of scintillations is then proportional to

$$1/\tau_{\text{abs}} = (1/\tau_{\text{He}})(1 - P_{\text{UCN}} \cdot P_3). \quad (3.8)$$

For the relaxation to be dominated by the ^3He (so $\tau_{\text{He}} = \tau_{\beta}/10$), $N_3 \approx 10^{13}/\text{cm}^3$ is required. This implies, for an anticipated 30 ℓ storage vessel with a 1000 s measurement period, and a fill time of 500 s (total polarized ^3He collection time of 1500 s), a polarized ^3He production rate of 2×10^{14} atoms/s if the ^3He is renewed after each measurement cycle.

3.4. Polarization of ^3He

The idea of using the strong spin dependence of neutron absorption by ^3He to polarize neutrons has been around for some time [Passell and Schermer 1960]. The problem is to produce a high ^3He polarization at a sufficiently high density and is discussed in detail in Coulter et al. [1987] in regard to application to relatively high-energy (1 eV) neutrons. There are several methods of producing polarized ^3He presently available.

Cryogenic methods, involving the melting of polarized solid ^3He produced at mK temperatures (see Vermeulen and Frossati [1987] and references therein). These techniques seem too specialized for the average neutron laboratory.

Two optical pumping methods which have been under active development for several years. The first consists of directly pumping a gas of metastable ^3He atoms (produced by an electrical discharge) with light from an LNA laser. This technique has produced between 20% [Milner et al. 1989] and 70% [Nachor et al. 1982; Aminoff et al. 1989] polarization. The second method produces polarized ^3He by spin-exchange collisions with optically pumped rubidium vapor (see Coulter et al. [1987] and references therein). This method has also produced 70% ^3He polarization. In the above work, emphasis was on producing a high density of adequately polarized ^3He for use as a polarizer with high-energy neutrons. However, for our proposed new technique to search for the neutron EDM, the polarized ^3He density need not be so high, while the polarization must be very near one (as shown in section 3.6, the sensitivity is a strong function of the ^3He polarization).

For our purposes, the most interesting method to produce polarized ^3He , offering the possibility of higher polarization than methods based on optical pumping, is to use a magnetic hexapole to preferentially focus one of the ^3He spin states in an atomic beam. In a cylindrical hexapole magnetic field, particles with a magnetic moment experience a radial force

$$F_r = \pm \alpha r^2, \quad (3.9)$$

where the \pm refer to the two spin states. Under the influence of this force, one spin state is deflected out of the beam while the other undergoes two dimensional harmonic motion in the transverse plane. The most famous application of a similar technique (electric-quadrupole focussing of a molecular electric-dipole moment) was the production of a population inversion in the ammonia maser [Gordon et al. 1955] where it was estimated that 10^{15} molecules per second were selected in a solid angle of 4×10^{-3} sterad.

Following Ramsey [1956], for magnetic moments in a hexapole field, we find that the maximum angle which can be focussed is given by

$$\Theta_{\max} = \sqrt{\mu B/kT}, \quad (3.10)$$

where μ is the magnetic moment, B the maximum magnetic-field strength, T is the effective temperature of the atoms in the beam, and k is Boltzmann's constant. With a maximum field strength of 10^4 G and a beam temperature of 1 K, eq. (3.10) gives $\Theta_{\max} = 2 \times 10^{-2}$ rad, giving a focussed solid angle of

$$\Omega_f = \pi \Theta_{\max}^2 = 1.2 \times 10^{-3}. \quad (3.11)$$

Since an atom in the appropriate spin state undergoes harmonic motion in the transverse plane, the length of the focussing region must be such that one-half of an oscillation cycle takes place during the flight time, in which case the atom will have zero displacement from the beam axis at the end of the hexapole region and hence be focussed on the output aperture. This gives a length of the focussing region $L = \pi r_m / \Theta_{\max}$ where r_m is the maximum beam deviation from the axis (set by collimation and magnet design) and the radius at which B is measured. This gives $L = 126$ cm for $r_m = 1$ cm with the above-listed parameters.

The number of atoms per second leaving a source of area A into a solid angle Ω is given by

$$I = \frac{1}{4} n \bar{v} (\Omega/2\pi) A s^{-1}, \quad n = 4 \times 10^{16} P \times 300/T, \quad (3.12a, b)$$

where n is the atomic density, P is the source pressure in Torr, and \bar{v} is the average velocity of the atoms in the source (10^4 cm/s for ^3He at 1 K). By working at a source pressure of 10^{-2} Torr, we obtain $n = 1.2 \times 10^{17}/\text{cm}^3$ and

$$I \approx 3 \times 10^{15} \text{ atoms/s}, \quad (3.13)$$

using six sources of 1 mm^2 area each; this production rate is a factor of 5 greater than that required as discussed in section 3.3. Thus, it appears that we can produce enough polarized ^3He for the purposes of the present experiment. The actual performance of such a device will be determined by the details of the source orifice (e.g., Zacharias crinkly foils or micropores [King and Zacharias 1956; Scoles 1988]) and the number and type of differential pumping stages, but we would expect to achieve a very high polarization, limited only by the background ^3He in the vacuum system and spurious magnetic gradients at the hexapole output.

3.5. Detection of scintillations

The reaction $^3\text{He}(n, p)^3\text{T}$ yields 764 keV kinetic energy to the reaction products and should produce scintillations in the liquid ^4He . Studies of the light produced in liquid ^4He by α particles [Roberts and Hereford 1973; Hereford and Moss 1969] or energetic electrons [Stockton et al. 1970; Surko et al. 1970] or neutrons have shown scintillations at ultraviolet [Stockton et al. 1970; Surko et al. 1970] and infrared wavelengths [Dennis et al. 1969] and in the visible in the presence of an oxygen impurity [Jortner et al. 1964]. The highest intensity appears to be in the vacuum ultraviolet; the ultraviolet emission is detected by coating the helium chamber or a window with an organic "wavelength shifter" which emits visible light on absorbing the uv radiation.

For reasons of UCN compatibility we would have to use deuterated versions of these wavelength shifters, or a very low concentration of an organic dye in a deuterated carrier. On the other hand if oxygen coating on the walls could serve as a wavelength shifter the problem would be considerably simplified. The scintillations produced by α particles and high-energy neutrons have been shown to result in a quite well defined pulse-height spectrum [Simmons and Perkins 1961]. The extension of these results to the ionization produced by neutron absorption by ^3He and the related question of γ -ray discrimination remain to be investigated.

3.6. ^3He as a comagnetometer

From eq. (3.8) we write the scintillation rate,

$$S(t) = (\rho_{\text{UCN}} V / \tau_{\text{He}}) [1 - P_n P_3 \cos \theta_{n3}(t)], \quad (3.14)$$

with $\theta_{n3}(t)$ the angle between the UCN and ^3He spins and V the total volume. If both the neutron and ^3He spins are precessing in a plane perpendicular to an applied magnetic field, we will have

$$\theta_{n3}(t) = (\gamma_n - \gamma_3)B_0 t = \omega_{\text{rel}} t, \quad \gamma_3 \approx 1.1\gamma_n \quad (3.15)$$

so that the scintillations will be modulated at a frequency

$$\omega_{\text{eff}} \approx 0.1\gamma_n B_0 \quad (3.16)$$

at 1/10 of the normal Larmor frequency. A neutron EDM would manifest itself as the addition of a field-dependent term ($\pm 2ed_n Et/\hbar$) to eq. (3.15) and could be detected by monitoring the scintillation rate.

However, we see below that there are still more tricks that can be played with this unique system of two spin species interacting according to eq. (3.8).

3.7. Elimination of the effects of the dc magnetic field by means of “critical dressing”

3.7.1. Dressed-spin technique

“Dressed spin” is a term that has been applied to the phenomenon of the apparent change in the magnetic dipole moment caused by the application of a high-frequency nonresonant alternating magnetic field [Cohen-Tannoudji and Haroche 1969].

The effect can be understood with the following simple model: Consider a spin, initially pointing along the z axis. On application of a field

$$B_x(t) = B_{\text{rf}} \sin \omega_{\text{rf}} t \quad (3.17)$$

the spin will precess in the y - z plane with a frequency

$$\omega(t) = \gamma B_x(t) = \dot{\theta}(t), \quad (3.18)$$

so that the angle, θ , with the z axis will be given by

$$\theta(t) = \gamma(B_{\text{rf}}/\omega_{\text{rf}}) \cos \omega_{\text{rf}} t. \quad (3.19)$$

Thus the time average of the z component of the spin will be

$$\langle \cos \theta(t) \rangle_T = \frac{1}{T} \int_T dt \cos [(\gamma B_{\text{rf}}/\omega_{\text{rf}}) \cos \omega_{\text{rf}} t] = J_0(\gamma B_{\text{rf}}/\omega_{\text{rf}}) \equiv J_0(x), \quad (3.20)$$

with x defined as the dressing parameter. The spin will thus respond to a small field along the z axis with an effective γ

$$\gamma_{\text{eff}} = \gamma_0 J_0(x). \quad (3.21)$$

The effect has been demonstrated experimentally with a beam of slow neutrons [Muskat et al. 1987].

3.7.2. Critical dressing

If we apply a dressing field to the case discussed in subsection 3.6, i.e. the neutron and ^3He spins precessing in a constant magnetic field, the relative precession rate (3.15) will become

$$\omega_{\text{rel}} = (\gamma_n^{\text{eff}} - \gamma_3^{\text{eff}})B_0 ; \quad \gamma_i^{\text{eff}} = J_0(x_i)\gamma_i , \quad x_i = \gamma_i B_{\text{rf}}/\omega_{\text{rf}} , \quad i = \text{UCN}, ^3\text{He} . \quad (3.22)$$

We now see that we can eliminate the effect of the magnetic field B_0 if

$$\gamma_n J_0(x_n) - \gamma_3 J_0(x_3) = 0 , \quad \gamma_3/\gamma_n = x_3/x_n \approx 1.112 = \alpha \quad (3.23)$$

i.e.,

$$\alpha J_0(\alpha x_c) = J_0(x_c) , \quad (3.24)$$

which has a solution at the ‘‘critical’’ dressing parameter

$$x_c \approx 1.19 , \quad J_0(x_c) = 0.65 . \quad (3.25)$$

Under these conditions the scintillation rate would be constant, independent of the DC magnetic field, correct up to terms of order $(B_0/B_{\text{rf}})^2$ which can be shown to have no significant effects on the following discussion.

3.8. Applications of critical dressing to the search for a neutron EDM

In the presence of a nonzero EDM, application of an electric field to the case with critical dressing will result in a relative precession frequency

$$\omega_{\text{rel}} = \pm(2ed_n E/\hbar)J_0(x_c) , \quad (3.26)$$

so that the angle between the UCN and ^3He will grow with time as

$$\theta_{n3} = \omega_{\text{rel}}t = \pm 2e\tilde{d}_n Et/\hbar , \quad \tilde{d}_n = d_n J_0(x) , \quad (3.27)$$

and would be observable in the scintillation rate. The measurement can be carried out by starting with the UCN and ^3He spins parallel so that the absorption rate would be zero in the case of perfect polarization (or minimum in the case of imperfect polarization). If we then modulate the dressing field so that

$$x(t) = x_c + \varepsilon \cos \omega_m t , \quad (3.28)$$

we will have

$$\omega_{\text{rel}} \sim \varepsilon \cos \omega_m t \pm k\tilde{d}_n E , \quad (3.29)$$

or

$$\delta\theta \sim (\varepsilon/\omega_m)\sin \omega_m t \pm k\tilde{d}_n Et \sim \delta\theta_o(t) \pm k\tilde{d}_n Et , \quad (3.30)$$

with k a constant. In these circumstances the scintillation rate $S \propto (\delta\theta)^2$, and in the absence of an EDM will only show a second harmonic $\propto (\delta\theta_0)^2$. An EDM will then produce a first harmonic term increasing linearly in time. The second harmonic can provide a continuous monitoring of the system.

A more detailed analysis, presented in section 6, shows that the statistical accuracy in terms of UCN counted, storage time, and electric field, is roughly the same as the conventional method using Ramsey's method of separated oscillatory fields. Thompson [1992] has presented an analysis of a similar, but simplified system which does not include the modulation technique and neglects several other of the important features which we will discuss in sections 5 and 6.

4. Quantum analysis of the dressed spin system

4.1. Constant magnetic field as perturbation on the eigenstates of the spin in an oscillating field

The problem of a dressed spin has been treated quantum mechanically by Cohen-Tannoudji and Haroche [1969] (see also Polonsky and Cohen-Tannoudji [1965]). In this section, we review their work and apply the result to the case of two spins mutually absorbing according to eq. (3.8) (section 3.3). We then consider the effects of imperfect alignment of the constant magnetic field and higher-order perturbations.

The Hamiltonian for a spin-1/2 particle with gyromagnetic ratio γ located in a steady magnetic field B_0 along z and a quantized oscillating magnetic field (at frequency ω) along x is given by

$$H = \omega a^\dagger a + \gamma(2\pi\hbar\omega)^{1/2} s_x (a + a^\dagger) + \omega_0 s_z, \quad (4.1)$$

where the first term represents the energy of the oscillating field, the second term the interaction of the spin with the oscillating field, and the third term the interaction energy of the spin with the constant field ($\omega_0 = \gamma B_0$). An eigenstate of the oscillating field corresponding to n photons corresponds to a magnitude of the oscillating field

$$(B_1^{\text{ms}})^2 = 4\pi n\hbar\omega/L^3 = B_1^2/2, \quad (4.2)$$

where B_1 is the "peak" of the oscillating field when viewed as a classical field.

Following Cohen-Tannoudji and Haroche [1969], we treat the last term in eq. (4.1) as a perturbation ($B_0 \ll B_1$). The unperturbed eigenstates are

$$\begin{aligned} \overline{|n, m_x\rangle} &= \exp[-(\lambda s_x/\omega)(a^\dagger - a)] |n\rangle |m_x\rangle \\ &= \exp[-(\lambda m_x/\omega)(a^\dagger - a)] |n\rangle |m_x\rangle = \overline{|n_{m_x}\rangle} |m_x\rangle, \end{aligned} \quad (4.3)$$

where $|m_x\rangle$ is an eigenstate of s_x with eigenvalue m_x , $|n\rangle$ is an eigenstate of $a^\dagger a$ with eigenvalue n and energy eigenvalue

$$E_{n, m_x} = n\omega - m_x^2 \lambda^2/\omega, \quad \lambda = \gamma(2\pi\hbar\omega/L^3)^{1/2} \quad (4.4a, b)$$

so that the states $m_x = \pm 1/2$ are degenerate. The eigenstates $\overline{|n_{m_x}\rangle}$ defined in eq. (4.3) satisfy

$$\begin{aligned} \overline{\langle n_{+1/2} | (n-q)_{-1/2} \rangle} &= \langle n | \exp[(\lambda/\omega)(a^\dagger - a)] | (n-q) \rangle \\ &= J_q(2\lambda\sqrt{n/\omega}) = J_q(\omega_1/\omega), \end{aligned} \quad (4.5)$$

where $\omega_1 = \gamma B_1$ and $J_q(x)$ is the Bessel function of the first kind of order q . Polonsky and Cohen-Tannoudji [1965] obtained eq. (4.5) by expanding the exponential operator in a series and showing that the series obtained is equivalent to the expansion for the Bessel function in the case when $n, n-q \gg \omega_1/\omega$.

Since the states given in eq. (4.3) are degenerate for a fixed n , we calculate the effects of the perturbation $\omega_0 s_z$ by calculating its matrix elements in the basis eq. (4.3),

$$\begin{aligned} \overline{\langle m'_x, n | \omega_0 s_z | n, m_x \rangle} &= \langle m'_x | s_z | m_x \rangle \overline{\langle n_{m'_x} | n_{m_x} \rangle} \omega_0 \\ &= \langle m'_x | s_z | m_x \rangle \langle n | \exp[(m'_x - m_x)(\lambda/\omega)(a^\dagger - a)] | n \rangle \omega_0 \\ &= \langle m'_x | s_z | m_x \rangle J_0((m'_x - m_x)\omega_1/\omega) \omega_0, \end{aligned} \quad (4.6)$$

where the last step follows from eq. (4.5) and the fact that only $m'_x = m_x \pm 1$ because of the selection rules on s_z . Since $J_0(x) = J_0(-x)$, eq. (4.6) is diagonalized by transforming the eigenstates of s_x , $|m_x\rangle$ to the eigenstates of s_z , $|m_z\rangle$ and the perturbed energy levels are thus shifted from eq. (4.4a) by

$$\omega_d m_z = \omega_0 J_0(\omega_1/\omega) m_z, \quad (4.7)$$

the factor $J_0(\omega_1/\omega)$ representing the modification of the magnetic moment by “dressing”. In the presence of an EDM interaction, ω_0 in eqs. (4.1) and (4.7) will be replaced by $\omega_0 + 2dE/\hbar$ so that the EDM will be diluted by the dressing in the same way as the magnetic moment as assumed in eq. (3.21).

Henceforth, we will find it more convenient to work in the $\sigma = 2s$ basis ($m = 2m_z = +$ or $-$). The correct eigenstates of the Hamiltonian eq. (4.1) are

$$\overline{|n, m\rangle} = \alpha \overline{|n_+\rangle} |+\rangle_x + \beta \overline{|n_-\rangle} |-\rangle_x, \quad (4.8)$$

where α and β are determined by the value of m . In our original $|m_x\rangle$ representation, we have

$$\sigma_x = \begin{pmatrix} 1 & 0 \\ 0 & -1 \end{pmatrix}, \quad \sigma_y = \begin{pmatrix} 0 & 1 \\ 1 & 0 \end{pmatrix}, \quad \sigma_z = \begin{pmatrix} 0 & -i \\ i & 0 \end{pmatrix}, \quad (4.9)$$

and the m_z eigenstates can be written

$$\overline{|n, m\rangle} = (1/\sqrt{2})(\overline{|n_+\rangle} |+\rangle_x + im \overline{|n_-\rangle} |-\rangle_x), \quad (4.10)$$

with energy given by $n\omega + m\omega_d/2 - m^2\lambda^2/4\omega$. The last term is a constant shift for all levels and so does not contribute to the time dependence.

4.2. Time dependence of $\langle \sigma \rangle$

We take an initial state with $\langle \sigma \rangle$ pointing along the x axis and a superposition of n values corresponding to a classical field B_1 . We first consider the matrix elements of σ between states with quantum numbers n and n' , with $q = n - n'$. Using eq. (4.10), we calculate the matrix elements of σ_x in the basis of the eigenstates eq. (4.8),

$$\begin{aligned} & \exp[-i(n'\omega + \frac{1}{2}m'\omega_d)t] \overline{\langle n', m' | \sigma_x | n, m \rangle} \exp[i(n\omega + \frac{1}{2}m\omega_d)t] \\ &= \frac{1}{2} [\overline{\langle n'_+ | n_+ \rangle} - im'(im)(-1)\overline{\langle n'_- | n_- \rangle}] \exp\{i[(n - n')\omega + \frac{1}{2}(m - m')\omega_d]t\} \\ &= \delta_{n,n'} \frac{1}{2}(1 - m'm) \exp[\frac{1}{2}(m - m')\omega_d t] \\ &= \begin{cases} 0, & m = m', \\ \delta_{n,n'} \exp[i\frac{1}{2}(m - m')\omega_d t], & m \neq m'. \end{cases} \end{aligned} \quad (4.11)$$

Taking an initial state with spin along the $+x$ axis,

$$\psi(t) = \sum_{n,m=\pm 1} a_n (1/\sqrt{2}) \overline{|n, m\rangle} \exp[it(n\omega + \frac{1}{2}m\omega_d)], \quad (4.12)$$

we find the time dependence of the expectation value of σ_x ,

$$\langle \psi(t) | \sigma_x | \psi(t) \rangle = \langle \sigma_x(t) \rangle = \sum_{n,n'} a_n^* a_n \delta_{n,n'} \cos \omega_d t = \sum_n |a_n|^2 \cos \omega_d t = \cos \omega_d t, \quad (4.13)$$

since $\sum_n |a_n|^2 = 1$. Similarly, for σ_y , the matrix elements between eigenstates are

$$\begin{aligned} & \exp[-i(n'\omega + \frac{1}{2}m'\omega_d)t] \overline{\langle n', m' | \sigma_y | n, m \rangle} \exp[i(n\omega + \frac{1}{2}m\omega_d)t] \\ &= \exp(iq\omega t) \exp[i\frac{1}{2}(m - m')\omega_d t] J_{-q}(\omega_1/\omega) im \frac{1}{2} [1 - m'm(-1)^q], \end{aligned} \quad (4.14)$$

where we have used eq. (4.5) and the fact that $J_q(-x) = (-1)^q J_q(x)$. For q even (odd), the only nonzero matrix elements have $m' \neq m$ ($m' = m$). To evaluate the expectation value of σ_y using eq. (4.12), we first sum over $m = \pm 1$ and then for every pair of n, n' we have a term in $\pm q$. Thus

$$\begin{aligned} \langle \sigma_y(t) \rangle &= -J_0(\omega_1/\omega) \sin \omega_d t \\ &\quad - \sum_{q>0, \text{even}} \sum_n a_n a_{n-q}^* \{ J_q(\omega_1/\omega) [\sin(q\omega + \omega_d)t + \sin(\omega_d - q\omega)t] \}. \end{aligned} \quad (4.15)$$

Similarly,

$$\langle \sigma_z \rangle = \sum_{q>0, \text{odd}} \sum_n a_n a_{n-q}^* J_q(\omega_1/\omega) [\cos(q\omega - \omega_d)t - \cos(q\omega + \omega_d)t]. \quad (4.16)$$

Thus we see that $\langle \sigma_x \rangle$ behaves as if the spin were precessing around the constant field B_0 with a “dressed” frequency ω_d given by eq. (4.7) while the motion of $\langle \sigma_y \rangle$ and $\langle \sigma_z \rangle$ contain harmonics of the applied alternating field.

4.3. Time dependence of $\sigma_n \cdot \sigma_3$

In a system consisting of polarized UCN interacting with polarized ^3He the absorption (scintillation) rate is given by eq. (3.8). We now use the results of the previous section to calculate the time dependence of $\langle \sigma_n \cdot \sigma_3 \rangle$ starting in an initial state consisting of a product state of eq. (4.12) for the UCN and a similar state for the ^3He . Then

$$\langle \sigma_n \cdot \sigma_3 \rangle = \langle \sigma_n \rangle \cdot \langle \sigma_3 \rangle. \quad (4.17)$$

Thus, from eq. (4.13),

$$\langle \sigma_{3x} \sigma_{nx} \rangle = \cos \omega_n t \cos \omega_3 t = \frac{1}{2} [\cos(\omega_n - \omega_3)t + \cos(\omega_n + \omega_3)t], \quad (4.18)$$

where we have written $\omega_{n,3}$ for the UCN and ^3He dressed frequencies, eq. (4.7). We further define $x_{n,3} = \gamma_{n,3} B_1 / \omega$.

From eq. (4.15) and given $\sum_n |a_n|^2 = 1$, $q \ll n$ and assuming a_n is a slowly varying function of n , we find

$$\begin{aligned} \langle \sigma_{3y} \sigma_{ny} \rangle &= \sum_{q, q' \geq 0, \text{ even}} J_q(x_n) J_q(x_3) [\sin(\omega_n + q\omega)t + \sin(\omega_n - q\omega)t] \\ &\quad \times [\sin(\omega_3 + q'\omega)t + \sin(\omega_3 - q'\omega)t] \end{aligned} \quad (4.19)$$

(where it is understood that we take 1/2 of the 0 terms) which yields for the zero harmonic, i.e., those terms which remain after averaging over the fast frequencies $q\omega$ ($q \geq 1$),

$$\begin{aligned} \langle \sigma_{3y} \sigma_{ny} \rangle &= \frac{1}{2} [\cos(\omega_n - \omega_3)t - \cos(\omega_n + \omega_3)t] \\ &\quad \times \left(J_0(x_n) J_0(x_3) + 2 \sum_{q > 0, \text{ even}} J_q(x_n) J_q(x_3) \right). \end{aligned} \quad (4.20)$$

Similarly, starting with eq. (4.16) we find the zero harmonic terms

$$\langle \sigma_{3z} \sigma_{nz} \rangle = [\cos(\omega_n - \omega_3)t - \cos(\omega_n + \omega_3)t] \sum_{q > 0, \text{ odd}} J_q(x_n) J_q(x_3). \quad (4.21)$$

Using Abramowitz and Stegun [1972],

$$J_0(x - y) = J_0(x) J_0(y) + 2 \sum_{k > 0} J_k(x) J_k(y) \quad (4.22)$$

we finally arrive at

$$\langle \sigma_3 \cdot \sigma_n \rangle = \frac{1}{2} [1 + J_0(x_n - x_3)] \cos(\omega_n - \omega_3)t + \frac{1}{2} [1 - J_0(x_n - x_3)] \cos(\omega_n + \omega_3)t, \quad (4.23)$$

for the zero harmonic terms. $J_0(x_n - x_3) > 0.99$ for x_n, x_3 in the neighborhood of x_c , the solution of eq. (3.23). We have thus shown that the time dependence of the scintillation rate is given by eq. (3.22), substituted in eqs. (3.15) and (3.14), and justified eq. (3.23) for the condition of critical

dressing. Note that the second term in eq. (4.23) is small and varies at twice the precession frequency so will average to zero in a practical experiment.

4.4. Effect of an x component of the static magnetic field

We now consider the case when the static magnetic field B_0 is not exactly perpendicular to the alternating field, taken as along the x axis. To do this, we replace the last term in the Hamiltonian (eq. 4.1) by

$$H' = \omega_0^z s_z + \omega_0^x s_x, \quad (4.24)$$

and evaluate the matrix elements of this operator in the eigenstates (eq. 4.3) of the unperturbed problem. Considering only matrix elements between degenerate states we find

$$\overline{\langle n, m'_x | H' | n, m_x \rangle} = \frac{1}{2} \begin{pmatrix} \omega_0^x & -i\omega_d^z \\ i\omega_d^z & -\omega_0^x \end{pmatrix}, \quad (4.25)$$

with ω_d^z given by eq. (4.7). Diagonalizing this matrix we arrive at the new first-order eigenvalues,

$$E^{(1)} = \pm \frac{1}{2} \sqrt{(\omega_0^x)^2 + (\omega_d^z)^2}. \quad (4.26)$$

Thus to maintain the critical dressing in the presence of a nonzero B_0^x we must have $E_n^{(1)} = E_3^{(1)}$ so that the UCN and ^3He will continue to precess at the same frequency. This yields the condition

$$(\alpha^2 - 1)(\omega_0^x/\omega_0^z)^2 = [J_0(x_n)]^2 - [\alpha J_0(\alpha x_n)]^2; \quad \alpha = \gamma_3/\gamma_n \quad \omega_0^{x,y} = \gamma_n B_0^{x,y}. \quad (4.27)$$

The right-hand side of eq. (4.27) is zero at $x_n = x_c = 1.189$, i.e., the solution of eq. (3.23). Expanding the r.h.s. about this point and writing the solution of eq. (4.27) as $x'_c = x_c + \delta$, we find

$$\delta = \frac{1}{2} \frac{(\alpha^2 - 1)(\omega_0^x/\omega_0^z)^2}{\alpha^2 J_0(\alpha x_c) J_1(\alpha x_c) - J_0(x_c) J_1(x_c)} = 1.94 \left(\frac{\omega_0^x}{\omega_0^z} \right)^2, \quad (4.28)$$

so that a minimum value of x_c will indicate that the B_0 field is truly perpendicular to the oscillating field $B_0^x = 0$ and a small misalignment (or random or systematic variation along this axis) will only affect x_c in second order. Thus, we have a reliable way to set $B_0^x = 0$, and for the rest of our discussion we assume the static field is perpendicular to the oscillating field and $\gamma B_0^z = \omega_0$.

4.5. Effect of variation of the static field

We can use the states given in eq. (4.10) (which diagonalize the Hamiltonian) to determine the higher-order corrections to the eigenvalues. States of different n are connected by the Hamiltonian of eq. (4.1), corresponding to the creation or annihilation of q photons by the motion of the spin. Using eqs. (4.5) and (4.10), we can determine the matrix elements of the perturbation in the eigenstates of the unperturbed Hamiltonian,

$$V_{(n+q, m'), (n, m)} = \overline{\langle n+q, m' | \frac{1}{2} \omega_0 \sigma_z | n, m \rangle} = \frac{1}{4} \omega_0 [\text{im} J_q(\omega_1/\omega) - \text{im}' J_q(\omega_1/\omega)]. \quad (4.29)$$

The second-order correction to the energy is given by (remembering that the zero-order states are degenerate in m)

$$E_{n,m}^{(2)} = \sum_{n',m'; n' \neq n} \frac{V_{(n,m),(n',m')} V_{(n',m'),(n,m)}}{E_n^{(0)} - E_{n'}^{(0)}}. \quad (4.30)$$

Substituting the matrix elements from eq. (4.29) we find, after summing over m'

$$E_{n,m}^{(2)} = \frac{1}{8} \frac{(\omega_0)^2}{\omega} \sum_{q \neq 0} \frac{J_q^2(\omega_1/\omega)}{q} = 0, \quad (4.31)$$

since the sum extends over all $\pm q \neq 0$.

The third-order corrections to the eigenvalues are given by

$$E_{n,m}^{(3)} = -V_{(n,m),(n,m)} \sum_{n',m'} \frac{|V_{(n',m'),(n,m)}|^2}{(E_n^{(0)} - E_{n'}^{(0)})^2} + \sum_{n'',m''} \sum_{n',m'} \frac{V_{(n,m),(n'',m'')} V_{(n'',m''),(n',m')} V_{(n',m'),(n,m)}}{(E_n^{(0)} - E_{n''}^{(0)})(E_n^{(0)} - E_{n'}^{(0)})}. \quad (4.32)$$

Since the two terms above are of comparable magnitude and the second is much more complicated, we evaluate only the first term. Thus,

$$E_{n,m}^{(3)} \approx -m \frac{1}{8} J_0(\omega_1/\omega) \omega_0 \left(\frac{\omega_0}{\omega} \right)^2 \sum_{q=1}^{\infty} \frac{J_q^2(\omega_1/\omega)}{q^2}. \quad (4.33)$$

The shift in the eigenvalue $\delta E^{(3)}$ with a small change in the constant field δB is

$$\delta E^{(3)} \approx \frac{1}{2} (\omega_0/\omega)^2 \delta \omega_0, \quad \gamma(B_0 + \delta B) = \omega_0 + \delta \omega_0, \quad (4.34)$$

which is extremely small for the anticipated field values ($\omega_0/\omega \approx 1 \times 10^{-3}$). The change in critical dressing parameter, following a similar argument as in section 4.4 is of the order given by eq. (4.34). This implies that the change in x_c due to random or systematic field variations along B_0 will be insignificant.

It is also apparent that the direct effects of the applied static electric field cannot affect x_c other than through an EDM; there is no coupling of the electric field to the system constituents (photons or spin-1/2 particles) in eq. (4.1), other than through a possible EDM term for the neutron or for the ^3He which is expected to be small due to electron shielding. In fact in this experiment we will really be measuring the difference between the neutron and ^3He EDMs.

4.6. Numerical solution of free precession with rf and dc fields

The classical equation for the spin motion was solved numerically:

$$ds/dt = \gamma s \times \mathbf{B}, \quad \mathbf{B} = B_{rf} \cos \omega_{rf} t \hat{x} + B_0 \hat{z}, \quad (4.35a, b)$$

with $\omega_{\text{rf}}/2\pi \approx 10$ kHz and $\gamma B_0/2\pi \approx 5$ Hz, for each spin (UCN and ^3He) separately, and $s_n \cdot s_3$ was evaluated as a function of time. A fourth-order Runge–Kutta technique was used with about 20 steps over a single rf cycle. Thus, considerable computing time was required to generate 100 s of free precession. In addition, a model of the feedback technique described in section 5.4 was used to determine x_c , and shows that in principle the proposed technique works. However, since the numerical integration was quite lengthy, due to round-off errors only qualitative comparisons with the quantum solution can be made.

The harmonic series eqs. (4.20) and (4.21) were qualitatively verified. Most interesting, however, was the verification of the effect of higher-order perturbation and field misalignments on x_c [eqs. (4.28), (4.31) and (4.34)].

The dressed spin system is a vivid example of the power of quantum versus classical perturbation theory. It is obvious in this case that the quantum-mechanical perturbation works because the system can be described fully with the never-changing eigenfunctions; there is nothing analogous for the classical system. The solution of the spin-1/2 Bloch equations with arbitrary strength oscillating and static magnetic fields is an analytically difficult problem.

5. Interaction of UCN with ^3He

5.1. Introduction

The interaction of a neutron with a ^3He atom is described by a complex coherent scattering length, the imaginary part being necessary to account for the large absorption cross section. In our discussion, we have so far neglected the real part which leads to the so-called Abragam pseudomagnetic field [Abragam and Goldman 1982; Abragam et al. 1972]. Both the real and imaginary parts of the coherent scattering length are spin-dependent; therefore, there is a spin dependence of the Fermi potential [Foldy 1945; Steyerl 1977; Sears 1989; Ignatovich 1990; Golub et al. 1991] (real part) and a spin dependence of the UCN– ^3He absorption rate (imaginary part). The latter has already been described in section 3. The spin dependence of the real part of the scattering length leads to a spin-dependent Fermi potential which is indistinguishable from a magnetic field and has a magnitude of order 10^{-2} Hz for the anticipated ^3He density. This leads to a number of problems. First, the pseudomagnetic field is unlike an externally applied magnetic field in that the dressing does not eliminate its effects on the relative spin precession. Second, the pseudomagnetic field is perpendicular to the electric-field axis; the neutron spin precesses around the vector sum of the small EDM field and the much larger pseudomagnetic field. This leads to a reduction in the experimental sensitivity. In this section, we will determine the relative spin motion with the full neutron– ^3He interaction when the modulation of the dressing parameter as described in section 3.8 is applied.

The calculation is most readily carried out when the dressing-parameter modulation is a square wave. We assume that the spins are initially parallel. The dressing parameter is first shifted by a small amount x_m , giving a *relative* precession frequency between the ^3He and UCN spins of ω_z (equivalent to a magnetic field, which affects only the UCN spin, along \hat{z} in a frame rotating with the ^3He spin), $\omega_z = \gamma B_0 [J_0(x_c + x_m) - \alpha J_0(\alpha(x_c + x_m))]$ for a duration $\tau/2$. After this period, the dressing parameter is changed to $x_c - x_m$ giving a relative precession frequency of $-\omega_z$ for a duration τ . Thereafter, the dressing parameter is alternated giving $\pm\omega_z$, each with duration τ . The net effect is that the relative spin angle is triangle-modulated between $\pm\phi = \pm\omega_z\tau/2$, leading to a periodic variation in the scintillation signal at twice the modulation frequency ($2 \times 1/2\tau$). If

there is a relative precession between the spins (due to, e.g., an EDM), the relative spin angle will become asymmetric, with the asymmetry growing linearly in time as described in section 3.8. Thus, an EDM would produce a periodic variation in the scintillation signal, with frequency $1/2\tau$, and amplitude growing initially linearly in time but limited, however, by precession around the pseudomagnetic field as discussed below.

5.2. Time evolution of the UCN spin with modulated dressing

The neutron ^3He coherent and incoherent scattering lengths have been experimentally determined [Koester et al. 1991],

$$b_c = 5.73 - 1.483i \text{ fm}, \quad b_i = -2.5 + 2.568i \text{ fm},$$

which gives spin-dependent scattering lengths

$$b_+ = b_c + [I/(I+1)]^{1/2} b_i = 4.29 + 0i \text{ fm}$$

for the neutron and ^3He spins parallel, and

$$b_- = b_c - [(I+1)/I]^{1/2} b_i = 10.07 - 5.93i \text{ fm}$$

for the spins antiparallel. As we have already discussed, there is mutual absorption only when the spins are antiparallel. The difference in the real parts of b_+ and b_- gives the pseudomagnetic field which is coincidentally very nearly equal to the imaginary part of b_- . Thus, the relative spin-precession frequency is equal to the mutual absorption rate (for the spin antiparallel) to rather high accuracy.

As the number of ^3He atoms in the system is always much greater than the number of UCN we can take σ_3 as a classical field in the x direction. In addition, we take the modulation field in the $\pm z$ direction. The Hamiltonians for the relative motion of the two spin species [see eq. (4.23)] and the two directions of effective modulation field are

$$H_{\pm} = -\frac{1}{2}i[1/\tau_0 - (P_3/\tau_{\text{He}})\sigma_n \cdot \sigma_3] + AP_3\sigma_n \cdot \sigma_3 \pm \omega_z \sigma_z \cdot \hat{z}, \quad 1/\tau_0 = 1/\tau_{\text{w}\beta} + 1/\tau_{\text{He}}, \quad (5.1)$$

where A is the pseudomagnetic field. The total Hamiltonian for the system consists of the sum of eqs. (5.1) and (4.1). As eq. (5.1) is much smaller than the first two terms of eq. (4.1) we are effectively taking it as a perturbation. The time-averaged effects of eq. (4.1) are given by eq. (4.23). For eq. (5.1) we have

$$H_{\pm} = \frac{-i}{2\tau_0} \begin{pmatrix} 1 & 0 \\ 0 & 1 \end{pmatrix} + \begin{pmatrix} \pm\omega_z & P_3 A' \\ P_3 A' & \mp\omega_z \end{pmatrix}, \quad A' = A + \frac{i}{2\tau_{\text{He}}}, \quad (5.2)$$

with A' a complex quantity. The matrices are in the space of σ_n which we write as σ in the following. Then

$$\exp(-iH_{\pm}t) = \exp(-t/2\tau_0)[\cos Vt - i\sigma \cdot V(\sin Vt)/V], \quad V = \pm\omega_z \hat{z} + P_3 A' \hat{x}, \quad (5.3)$$

where \hat{z}, \hat{x} are unit vectors. Further we have

$$\exp(-iH_{\pm}t) = \exp(-t/2\tau_0) \begin{pmatrix} \cos Vt \mp i\omega_z S & -iP_3 A' S \\ -iP_3 A' S & \cos Vt \pm i\omega_z S \end{pmatrix}, \quad (5.4)$$

$$S = (\sin Vt)/V, \quad V^2 = \omega_z^2 + (P_3 A')^2 \approx \omega_z^2, \quad (5.5)$$

neglecting terms of order $\varepsilon^2 = (P_3 A'/\omega_z)^2$ which we will do from now on. Then

$$\exp(-iH_{\pm}t) = \exp(-t/2\tau_0) \begin{pmatrix} \exp(\mp i\omega_z t) & -i\varepsilon \sin \omega_z t \\ -i\varepsilon \sin \omega_z t & \exp(\pm i\omega_z t) \end{pmatrix}. \quad (5.6)$$

We apply the field $+\omega_z$ for time τ followed by the field $-\omega_z$ for time τ to produce one modulation period of length 2τ . Then

$$\begin{aligned} U_{-+}(2\tau) &= \exp(-iH_- \tau) \exp(-iH_+ \tau) \\ &= \exp(-\tau/\tau_0) \begin{pmatrix} 1 & -i2\varepsilon \exp(i\omega_z \tau) \sin \omega_z \tau \\ -i2\varepsilon \exp(-i\omega_z \tau) \sin \omega_z \tau & 1 \end{pmatrix} + O(\varepsilon^2) \\ &= \exp(-\tau/\tau_0) \begin{pmatrix} 1 & b \exp(i\omega_z \tau) \\ b \exp(-i\omega_z \tau) & 1 \end{pmatrix} = \exp(-\tau/\tau_0) (1 + b\sigma_i), \end{aligned} \quad (5.7)$$

$$b = -2i\varepsilon \sin \omega_z \tau = -2i(P_3 A'/\omega_z) \sin \omega_z \tau, \quad \sigma_i = \begin{pmatrix} 0 & \exp(i\omega_z \tau) \\ \exp(-i\omega_z \tau) & 0 \end{pmatrix},$$

where σ_i is a component of σ . After n periods we will have (see appendix A)

$$U_n \equiv [U_{-+}(2\tau)]^n = \left\{ \frac{1}{2}[(1+b)^n + (1-b)^n] + \frac{1}{2}[(1+b)^n - (1-b)^n] \sigma_i \right\} \exp(-n\tau/\tau_0). \quad (5.8)$$

Now

$$(1 \pm b)^n = \{1 \mp 2iP_3 A' [(\sin \omega_z \tau)/\omega_z \tau] \tau\}^n. \quad (5.9)$$

If we put $\tau = T/2n$ where T is the total elapsed time, using $(1 + x/n)^n \rightarrow e^x$ for $n \gg 1$, we can write,

$$(1 \pm b)^n \sim \exp[\mp iP_3 A' T (\sin \omega_z \tau / \omega_z \tau)] \equiv e^{\mp i\alpha}.$$

Then

$$U_n = \frac{1}{2} \exp(-T/2\tau_0) \begin{pmatrix} F_+ & F_- \exp(i\omega_z \tau) \\ F_- \exp(-i\omega_z \tau) & F_+ \end{pmatrix}, \quad (5.10)$$

$$F_{\pm} = [e^{-i\alpha} \pm e^{i\alpha}], \quad \alpha = bT/\tau. \quad (5.11)$$

Now we start with a modulation period of $\tau/2$ with the field in the minus direction so that the neutron spin will always be symmetric about σ_x . Then

$$\begin{aligned} U_{\text{tot}}(T) &= U_n \exp(-iH_- \tau/2) \\ &= \frac{1}{2} \exp(-T/2\tau_0) \begin{pmatrix} F_+ & F_- \exp(i\omega_z \tau) \\ F_- \exp(-i\omega_z \tau) & F_+ \end{pmatrix} \begin{pmatrix} \exp(i\omega_z \tau/2) & 0 \\ 0 & \exp(-i\omega_z \tau/2) \end{pmatrix} \\ &= \frac{1}{2} \exp(-T/2\tau_0) \begin{pmatrix} F_+ \exp(i\omega_z \tau/2) & F_- \exp(i\omega_z \tau/2) \\ F_- \exp(-i\omega_z \tau/2) & F_+ \exp(-i\omega_z \tau/2) \end{pmatrix}. \end{aligned} \quad (5.12)$$

For initial states $\psi_{\pm}(0) = (1/\sqrt{2}) \begin{pmatrix} 1 \\ \pm 1 \end{pmatrix}$ corresponding to the neutrons polarized parallel (anti-parallel) to the x axis we have

$$\psi_{\pm}(T) = U_{\text{tot}}(T) \psi(0) = \frac{\exp(-T/2\tau_0)}{2\sqrt{2}} (F_+ \pm F_-) \begin{pmatrix} \exp(i\omega_z \tau/2) \\ \pm \exp(-i\omega_z \tau/2) \end{pmatrix}, \quad (5.13)$$

$$\sigma_x \psi_{\pm}(T) = \frac{\exp(-T/2\tau_0)}{2\sqrt{2}} (F_+ \pm F_-) \begin{pmatrix} \pm \exp(-i\omega_z \tau/2) \\ \exp(i\omega_z \tau/2) \end{pmatrix}, \quad (5.14)$$

$$\langle \sigma_x \rangle = \psi_{\pm}^* \sigma_x \psi_{\pm} = \pm \frac{1}{4} \exp(-T/\tau_0) |F_+ \pm F_-|^2 \cos \omega_z \tau. \quad (5.15)$$

Now we have

$$\begin{aligned} (F_+ + F_-) &= 2e^{-i\alpha}, & (F_+ - F_-) &= 2e^{i\alpha}, \\ |F_+ + F_-|^2 &= 4 \exp[(P_3 T/\tau_{\text{He}})(\sin \omega_z \tau)/\omega_z \tau], \\ |F_+ - F_-|^2 &= 4 \exp[-(P_3 T/\tau_{\text{He}})(\sin \omega_z \tau)/\omega_z \tau], \\ -i\alpha &= [-iP_3 AT + (P_3 T/2\tau_{\text{He}})](\sin \omega_z \tau)/\omega_z \tau. \end{aligned} \quad (5.16)$$

Then

$$\langle \sigma_x \rangle_{\pm} = \pm \exp(-T/\tau_0) \exp[\pm (P_3 T/\tau_{\text{He}})(\sin \omega_z \tau)/\omega_z \tau] (\cos \omega_z \tau). \quad (5.17)$$

It can be seen that the neutron spin evolves according to the time average (over a modulation cycle) of the mutual interaction Hamiltonian. In this case the time dependence of $\langle \sigma_x \rangle$ is not affected by the Abragam term which is proportional to A . This should be compared to the case without modulated dressing discussed in appendix B. If we note that $\sin \omega_z \tau/\omega_z \tau$ is the time average of $\cos \theta_{n3}(t)$, the result eq. (5.17) with modulation shows classical behaviour in that there is only one decay constant for a given initial state while the familiar case of a time-dependent perturbation would show a ‘‘quantum’’ behaviour with a superposition of two decaying states.

The effect of the EDM is to replace $\omega_z^+ \rightarrow (\omega_z + \omega_e)$ and $\omega_z^- \rightarrow (-\omega_z + \omega_e)$. Then

$$|V_{\pm}|^2 = (\omega_z \pm \omega_e)^2 + (P_3 A')^2 = \omega_z^2 + (P_3 A')^2 \pm 2\omega_z \omega_e \quad (5.18)$$

[see eq. (5.3)]. We then find that eq. (5.6) is transformed to

$$\exp(-iH_{\pm}t) = \exp(-t/2\tau_0) \begin{pmatrix} \exp[\mp i(\omega_z \pm \omega_e)t] & -iP_3 A' S_{\pm} \\ -iP_3 A' S_{\pm} & \exp[\pm i(\omega_z \pm \omega_e)t] \end{pmatrix}, \quad (5.19)$$

so that

$$\begin{aligned} U_+(2\tau) &= e^{-iH-\tau} e^{-iH+\tau} \\ &= e^{-\tau/\tau_0} \begin{pmatrix} e^{-2i\omega_e\tau} - (P_3 A')^2 S_+ S_- & -iP_3 A' e^{i\omega_z\tau} [S_+ e^{-i\omega_e\tau} + S_- e^{i\omega_e\tau}] \\ -iP_3 A' e^{-i\omega_z\tau} (S_- e^{-i\omega_e\tau} + S_+ e^{i\omega_e\tau}) & e^{2i\omega_e\tau} - (P_3 A')^2 S_+ S_- \end{pmatrix} \\ &= e^{-\tau/\tau_0} \begin{pmatrix} e^{-2i\omega_e\tau} & -2i\epsilon e^{i\omega_z\tau} \sin \omega_z \tau \\ -2i\epsilon e^{-i\omega_z\tau} \sin \omega_z \tau & e^{2i\omega_e\tau} \end{pmatrix}. \end{aligned} \quad (5.20)$$

Thus

$$U_{-+}(2\tau) = e^{-\tau/\tau_0} \begin{pmatrix} e^{-2i\omega_e\tau} & b e^{i\omega_z\tau} \\ b e^{-i\omega_z\tau} & e^{2i\omega_e\tau} \end{pmatrix}. \quad (5.21)$$

Writing $\theta_e = 2\omega_e\tau$ we have

$$U_{-+}(2\tau) = e^{-\tau/\tau_0} \left[\begin{pmatrix} 1 & 0 \\ 0 & 1 \end{pmatrix} + \begin{pmatrix} -i\theta_e & b e^{i\omega_z\tau} \\ b e^{-i\omega_z\tau} & i\theta_e \end{pmatrix} \right] = e^{-\tau/\tau_0} [(1) + \boldsymbol{\sigma} \cdot \mathbf{V}], \quad (5.22)$$

where $(\sigma_v^2 = 1)$

$$\boldsymbol{\sigma} \cdot \mathbf{V} = \frac{\boldsymbol{\sigma} \cdot \mathbf{V}}{V} V = \sigma_v V = \begin{pmatrix} -i\theta_e & b e^{i\omega_z\tau} \\ b e^{-i\omega_z\tau} & i\theta_e \end{pmatrix}, \quad V^2 = b^2 - \sin^2 \theta_e \approx b^2. \quad (5.23a,b)$$

Now

$$U^n = e^{-n\tau/\tau_0} [(1) + V\sigma_v]^n. \quad (5.24)$$

Using the definition of b [given after eq. (5.7)] and putting $\cos \theta \approx 1$ [see definition of α after eq. (5.9)] we see that

$$(1 + b)^n = e^{-i\alpha}, \quad (1 + b)_{[\pm b]}^n = F_{\pm}. \quad (5.25)$$

where the subscript $[\pm b]$ refers to the odd and even parts (with respect to b). Then

$$U^n = \frac{1}{2} e^{-n\tau/\tau_0} [F_+(1) + (F_-/b)\boldsymbol{\sigma} \cdot \mathbf{V}], \quad (5.26)$$

$$U^n = \frac{1}{2} e^{-n\tau/\tau_0} \begin{pmatrix} F_+ - i(F_-/b)\sin \theta_e & F_- e^{i\omega_z\tau} \\ F_- e^{-i\omega_z\tau} & F_+ + i(F_-/b)\sin \theta_e \end{pmatrix}. \quad (5.27)$$

Since $iF_-/b = 2(\sin \alpha/\alpha)T/\tau$, we see a dilution of the EDM signal by a factor $\sin \alpha/\alpha$. This factor enters because the neutron spin precesses about the net field which includes both the EDM and the pseudomagnetic field. We will discuss methods to eliminate this effect in section 5.4.

It is now straightforward to work out the scintillation signal. We proceed to calculate σ_x from U^n (eq. 5.27) following the same procedure that led from eq. (5.10) to eq. (5.17). The result is that the scintillation rate per neutron is simply equal to the probability that the neutron exists at time T , multiplied by $1/\tau_{\text{abs}}$ [see eq. (3.8)]. The total rate is then proportional to N_0 , the initial UCN density. Defining R_{\pm} as the absorption rate for UCN originally in the state with $\sigma_x = \pm 1$,

$$R_{\pm} = \frac{N_0}{\tau_{\text{He}}} e^{-T/\tau_0} \left[e^{\pm\gamma T} \mp P_3 \left(e^{\pm\gamma T} \frac{\sin \omega_z \tau}{\omega_z \tau} \pm 2\omega_e T \eta_{\pm} \sin \omega_z \tau \right) \right], \quad (5.28)$$

where the second term represents the average scintillation rate due to the second harmonic and the third term the peak of the first harmonic, and

$$\eta_{\pm} = \frac{\gamma(e^{\pm\gamma T} - \cos \Omega T) + \Omega \sin \Omega T}{(\Omega^2 + \gamma^2)T},$$

$$\Omega = 2 \text{Re } \alpha, \quad \gamma = 2 \text{Im } \alpha, \quad \alpha = P_3 \frac{\sin \omega_z \tau}{\omega_z \tau} A',$$

$$A' = A + \frac{i}{2\tau_{\text{He}}}. \quad (5.29)$$

We arrive at the scintillation rate Φ ,

$$\begin{aligned} \Phi \tau_{\text{He}}/N_0 &= \frac{1}{2}(1 + P_0)R_+ + \frac{1}{2}(1 - P_0)R_- \\ &= \frac{1}{2}e^{-T/\tau_0} \left(e^{\gamma T} + e^{-\gamma T} - P_3 \frac{\sin \omega_z T}{\omega_z T} (e^{\gamma T} - e^{-\gamma T}) - 2\omega_e T P_3 \sin \omega_z \tau (\eta_+ + \eta_-) \right) \\ &\quad + \frac{1}{2}P_0 e^{-T/\tau_0} \left(e^{\gamma T} - e^{-\gamma T} - P_3 \frac{\sin \omega_z \tau}{\omega_z \tau} (e^{\gamma T} + e^{-\gamma T}) - 2\omega_e T P_3 \sin \omega_z \tau (\eta_+ - \eta_-) \right), \end{aligned} \quad (5.30)$$

$$\eta_+ - \eta_- = [\gamma(e^{\gamma T} - e^{-\gamma T}) + 2\Omega \sin \Omega T]/(\Omega^2 + \gamma^2)T \quad (5.31)$$

$$\eta_+ + \eta_- = \gamma(e^{\gamma T} + e^{-\gamma T} - 2 \cos \Omega T)/(\Omega^2 + \gamma^2)T. \quad (5.32)$$

It is evident that there is an EDM signal even in the absence of an initial UCN polarization ($P_0 = 0$). This is because the UCN become polarized during the measuring time. Also, the EDM signals are diluted by a factor $\eta_+ \pm \eta_-$ due to precession around the Abragam pseudomagnetic field.

5.3. Solution by use of the secular approximation

Since the frequency with which ω_z is modulated, $\omega_m = 2\pi/\tau$, is much larger than the other terms in (5.1) we are tempted to look for a solution using the secular approximation (see appendix B; Happer [1972] and Barrat and Cohen-Tannoudji [1961]). According to this approximation we can neglect rapidly varying terms in the equation for the time derivative of the density matrix if the magnitude of these terms is small compared to the modulation frequency. If we go into a reference frame which is always rotating with the Larmor frequency of the neutrons and, if the ^3He spins are in a plane perpendicular to the z axis, we will see the ^3He spins as making an oscillating motion about some axis (which we can take as the x axis) with a maximum amplitude $\omega_m\tau$. In this frame there will be no effective field along the z axis and the modulation frequency will be much larger than the magnitude of the terms in (5.1) depending on $\sigma_n \cdot \sigma_3$, so we can apply the secular approximation which yields

$$\langle \sigma_n \cdot \sigma_3 \rangle = \langle \cos \theta_{n3} \rangle, \quad (5.33)$$

where θ_{n3} is the angle between the spins. In the case of square-wave modulation of ω_z , $\langle \cos \theta_{n3} \rangle = (\sin \omega_z \tau) / \omega_z \tau$.

Note that if instead of the above procedure we chose to work in the reference frame rotating with the ^3He spins, as we did in section 5.2 above, we would have a nonzero component of ω_z which was rapidly modulated, but we would not be able to apply the secular approximation in this frame because $\omega_z/\omega_m = \omega_z \tau/\pi = \theta_m/\pi$ where θ_m is the maximum modulation angle and is not necessarily small compared to 1. By a similar argument, the secular approximation cannot be applied in the laboratory frame.

The calculation is most readily performed with the density matrix. At $T = 0$, we have

$$\rho(0) = \begin{pmatrix} (1 + P_0)/2 & 0 \\ 0 & (1 - P_0)/2 \end{pmatrix}. \quad (5.34)$$

The time dependence of the density matrix is given by

$$\rho(T) = U^\dagger(T)\rho(0)U(T), \quad U(T) = e^{-i\langle H \rangle T} \quad (5.35a, b)$$

and $\langle H \rangle$ is given by ($\langle \rangle$ represents the time average over many modulation cycles)

$$\langle H \rangle = -\frac{1}{2}i[1/\tau_0 - (P_3/\tau_{\text{He}})\langle \cos \theta \rangle \sigma_x] + AP_3 \langle \cos \theta \rangle \sigma_x + \omega_e \sigma_z, \quad (5.36)$$

where σ_z, σ_x refer to the neutron spin.

Equation (5.35b) can be expanded as shown in eq. (5.3) and it is straightforward to work out the expectation value of σ . The result of this calculation gives a scintillation rate equal to that derived above (eq. 5.30), with $(\sin \omega_z \tau) / \omega_z \tau$ replaced by $\langle \cos \theta \rangle$. We can thus use the result with any type of modulation; sinusoidal, square wave, pulse, etc., with the final choice based on ease of application and maximization of the signal-to-noise.

5.4. Elimination of the pseudomagnetic-field suppression by feedback to ω_z

A practical means of extracting the EDM signal is to keep the first harmonic zero by feeding back to the dressing parameter. By measuring the dressing parameter as a function of electric-field direction, the neutron EDM can be determined. In such a system, the calibration does not depend on the initial density, polarization, etc., which can vary between measurements.

The effects of feedback are most readily studied by use of the density-matrix approach outlined in section 5.3. To illustrate the method, we first consider a system where there is no UCN loss and the pseudomagnetic field has no imaginary component.

If the neutron and ^3He spins are parallel (along \hat{x}) and we apply a field which affects the neutron and ^3He spin differently, e.g., an electric field interacting with a neutron EDM, of magnitude $\omega_e < A$ along \hat{z} , the angle between the spins initially changes linearly in time; that is, the y projection of the neutron spin $s_y(t) = \omega_e t$, as is evident from eq. (5.3). It is only when $At \rightarrow 1$ that the $\sin \alpha/\alpha$ [see eq. (5.27)] suppression becomes significant. Furthermore, the modulation in essence serves as a measurement of the y component of the neutron spin, so long as on average the neutron spin lies approximately along \hat{x} , the ^3He spin. Since the first harmonic in the scintillation rate $\Phi_1 \propto s_y$, we can study the feedback by considering the behavior of s_y .

Since the applied field determines the rate of change of the relative spin angle, the UCN- ^3He system is mathematically equivalent to the voltage-controlled oscillator of a phase-locked-loop (PLL), with the first harmonic signal equivalent to the voltage output of the PLL phase detector; we can therefore design a feedback system based on the well-developed PLL techniques [Gardner 1979].

However, in our case, the feedback occurs only after successive modulation cycles. s_y is determined by the difference in scintillation rate between the two modulation directions, hence we can only supply a correction after a complete modulation cycle. This problem is difficult to attack analytically so we present here the result of a numerical simulation. (However, since the modulation frequency can be very high, the system can be modelled fully through the secular approximation; we perform the full calculation here to demonstrate the applicability of this approximation.)

The numerical procedure is as follows ($P_0 = 1$, $P_3 = 1$, the ^3He spin is fixed along \hat{x} and the scintillation rate is proportional to the \hat{x} projection of the neutron spin; consider first the case with no UCN loss, where A has no imaginary component):

```

Start: Set  $\omega_e$ ,  $A$ 
       $T = 0$ 
Loop:  $T = T + 2\tau$ 
       $\rho(T) = U_+^\dagger(\tau)\rho(T - \tau)U_+(\tau)$ 
       $\langle s_x \rangle_+ = \text{Tr}[\rho(T)s_x]$ 
       $\rho(T + \tau) = U_-^\dagger(\tau)\rho(T)U_-(\tau)$ 
       $\langle s_x \rangle_- = \text{Tr}[\rho(T + \tau)s_x]$ 
       $\omega_c = \omega_c - \alpha(\langle s_x \rangle_+ - \langle s_x \rangle_-)$ 
       $\omega_z = \omega_e + \omega_c - \beta(\langle s_x \rangle_+ - \langle s_x \rangle_-)$ 
      Go to Loop

```

In this procedure, $U_\pm(\tau)$ is as defined in eq. (5.19) with τ the modulation half-period, ω_c represents the correction to the applied \hat{z} field, α and β are effectively the constants in an integral plus proportional PLL feedback system, as shown schematically in fig. 7.

Results in the case $A = 0.06 \text{ s}^{-1}$ and $\omega_e = 0.01 \text{ s}^{-1}$ and very weak modulation [$(\sin \omega_z \tau)/\omega_z \tau = 0.99$] are shown in fig. 8. The values of the loop parameters α and β were

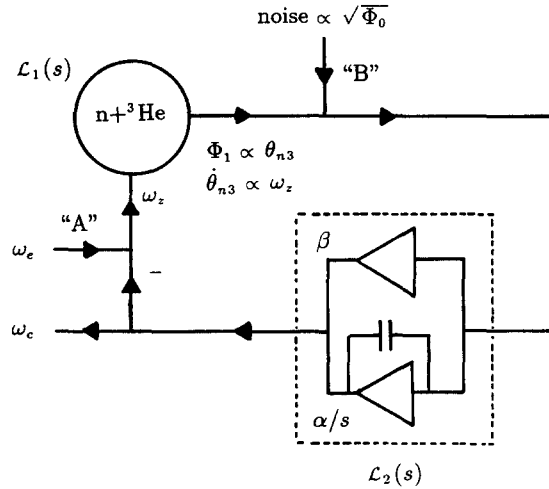


Fig. 7. Schematic of a feedback system following standard phaselock techniques. ω_z represents the total magnetic field seen by the UCN.

purposely chosen to give a very slow loop response ($\tau_L \approx 15$ s). There are a number of interesting points evident in the plots. First, the neutron spin must precess before there is a correction signal to be fed back on. During this time, the spin precesses around the vector sum of the fields and so no longer lies in the x - y plane. Referring to fig. 9, the neutron spin precesses about the net field at a frequency $\omega = (A^2 + \omega_e^2)^{1/2} \approx A$. The tip of the neutron spin moves along the circle of radius $r = \omega_e/A$ (for the magnitude of the spin vector $s = 1$) indicated in fig. 9, and in a time τ_L , moves a distance $rA\tau_L$. The final spin projection along the z axis, assuming no feedback before τ_L and rapid feedback after τ_L is

$$s_z \approx rA\tau_L(A\tau_L)/2 = \omega_e A\tau_L^2/2. \quad (5.37)$$

For the first harmonic to be held at zero (the system in an equilibrium state), the spin must lie along the final net field, that is,

$$s \parallel A\hat{x} + \omega'_z\hat{z}, \quad (5.38)$$

so in the final equilibrium state we have (for $s_z \ll 1$)

$$\omega'_z/A = s_z = \omega_e A\tau_L^2/2, \quad \omega'_z = \omega_e A^2\tau_L^2/2, \quad (5.39a, b)$$

which represents an error in the feedback signal (in an ideal system, the final value of ω_z should be zero). This effect is evident in fig. 8 where $\omega'_z \approx 1 \times 10^{-3}$. With the above-stated loop parameters, eq. (5.39b) gives $\omega'_z = 8 \times 10^{-4}$, in good agreement with the numerical-calculation result, particularly when the simple-minded loop model used in the derivation of eq. (5.39b) is considered.

The results of a full calculation including losses is given in fig. 10. In this case, $\tau_{\text{He}}^{-1} = 5\tau_{\text{wall}}^{-1} = 0.04 \text{ s}^{-1}$, $A = 0.02 - 0.02i \text{ s}^{-1}$, $P_3 = P_n = 1$ and $\omega_e = 1.0 \times 10^{-4}$ (again, weak modulation). After every 100 s, the sign of ω_e is reversed. The loop parameters were purposely chosen so that the loop is underdamped initially, however, as the effective system gain decreases with time (due to neutron loss), the loop becomes underdamped. Also plotted is the factor $\sin \alpha/\alpha$

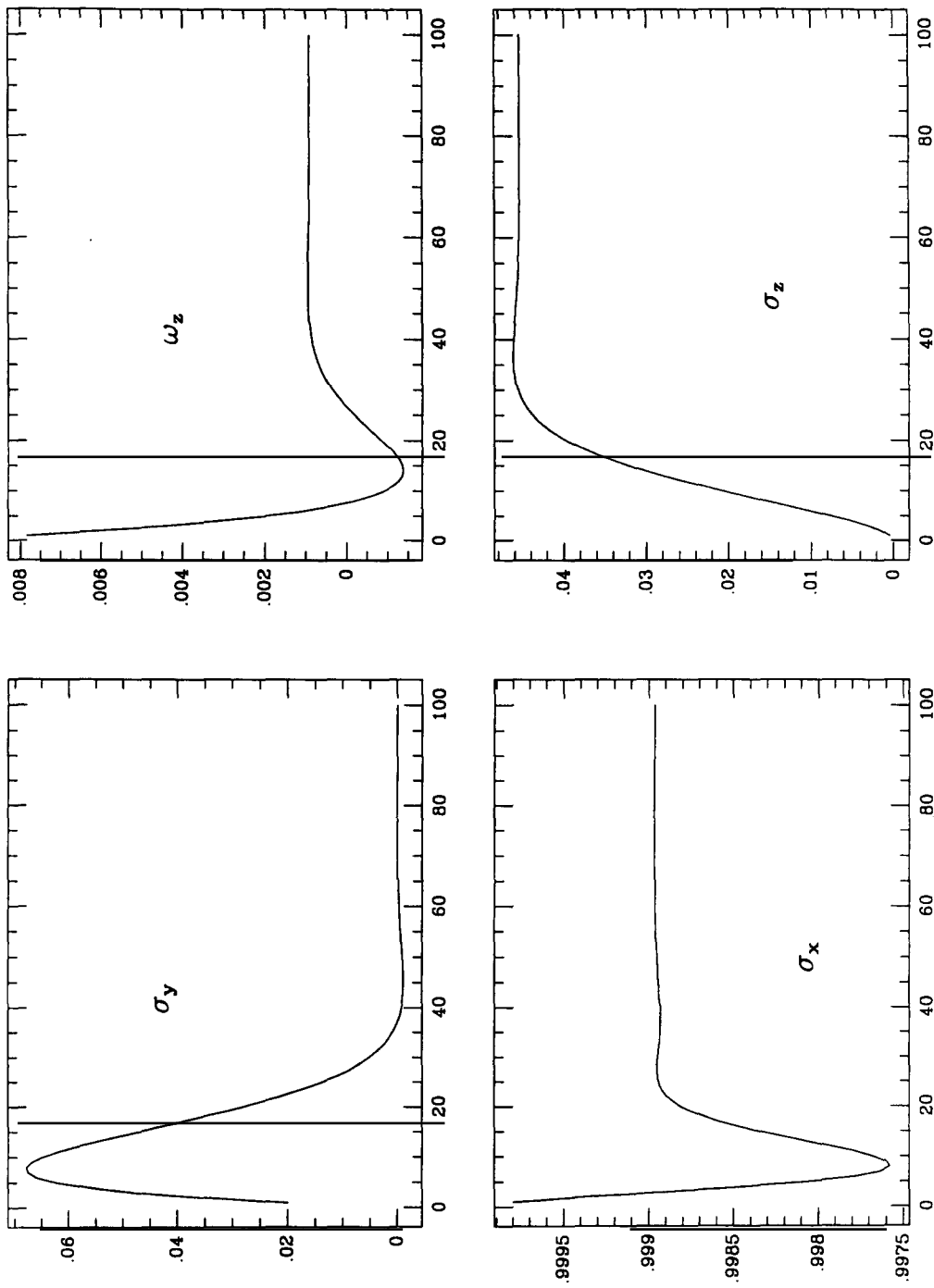


Fig. 8. Response of the system when τ_1 is rather long and with no UCN loss. The modulation period $\tau = 0.1$ s. The interesting feature is that $\omega_z \neq 0$, which implies that there is an error in the correction signal, after the system has reached equilibrium.

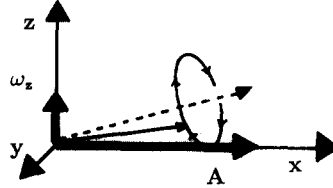


Fig. 9. Illustration of source of the feedback error due to the finite loop response time. The spin is initially along the x axis and precesses around the vector sum of the pseudomagnetic field along x and the magnetic field along z . In a time τ_L , the spin vector, initially along x , precesses out of the x - y plane by an angle $\phi \approx \omega_z A \tau_L^2 / 2$.

which illustrates the level of suppression of the EDM signal to be expected (for the electric field applied in a fixed direction) in a system without feedback. Clearly, this reduction factor is absent in the feedback response, and the correction signal, ω_c , accurately tracks ω_e . The results show that in the case of fast loop response and relatively small ω_e , the error in the feedback is very small.

It is evident from this analysis that feeding back to keep $s_y = 0$ (or, equivalently, keeping the first harmonic zero) eliminates the $\sin \alpha / \alpha$ suppression. An important advantage of the feedback technique is that the system is automatically calibrated; feedback by changing the dressing parameter (either ω_{rf} or B_{rf}) results in a directly measurable quantity, δx_c , which depends only on the applied dressing field and has a fixed calibration. The experimentally measured parameter which gives the EDM is the feedback correction signal as a function of electric-field polarity. Explicitly, from eqs. (3.20) to (3.23), with $\omega_0 = \gamma B_0$,

$$\omega_0 [J_0(x_c \pm \delta x_c) - 1.1 J_0(1.1(x_c \pm \delta x_c))] \pm 2e\tilde{d}_n E / \hbar \equiv 0, \quad (5.40)$$

which leads to

$$2\tilde{d}_n E / \hbar \approx \frac{1}{4} \omega_0 \delta x_c. \quad (5.41)$$

We point out that another technique to eliminate the effect of the $\sin \alpha / \alpha$ term is to set the modulation angle so that the average spin angle $\langle \cos \theta \rangle = 0$. In the case of square-wave modulation, this requires a maximum angular deviation (defined as θ_m) $\theta_m = \pi$. In the case of sinusoidal modulation, the maximum angle θ_m must satisfy $J_0(\theta_m) = 0$ where J_0 is the zero-order Bessel function, which interestingly is the same condition to eliminate the magnetic moment with rf dressing. This is to be expected as the effects of modulation of the spin orientation are the same as described in section 3.7 in regard to rf dressing, only the time scale is different.

5.5. Effects of the z component of the pseudomagnetic field

In practice it will be impossible to control the angle of the ^3He and neutron spins to better than 10^{-3} rad. Thus there can be a component of the pseudomagnetic field along \hat{z} of order $10^{-3} A$, and $A \leq 10^{-2}$ Hz, giving a relative shift of 10^{-5} Hz, which is a factor of 10 to 100 larger than the anticipated sensitivity per measurement period. This shift can vary between fillings and will be time-dependent as the ^3He polarization decays. Since the shift is independent of E , a possible way to contend with this problem is to vary the electric field periodically over the course of a measurement and to look for a correlation between the field polarity and feedback signal. Since the effects due to the external magnetic fields generated by charging or leakage currents are strongly suppressed [see eqs. (4.28) and (4.34)], the field-reversal rate could be relatively high (5–10 reversals

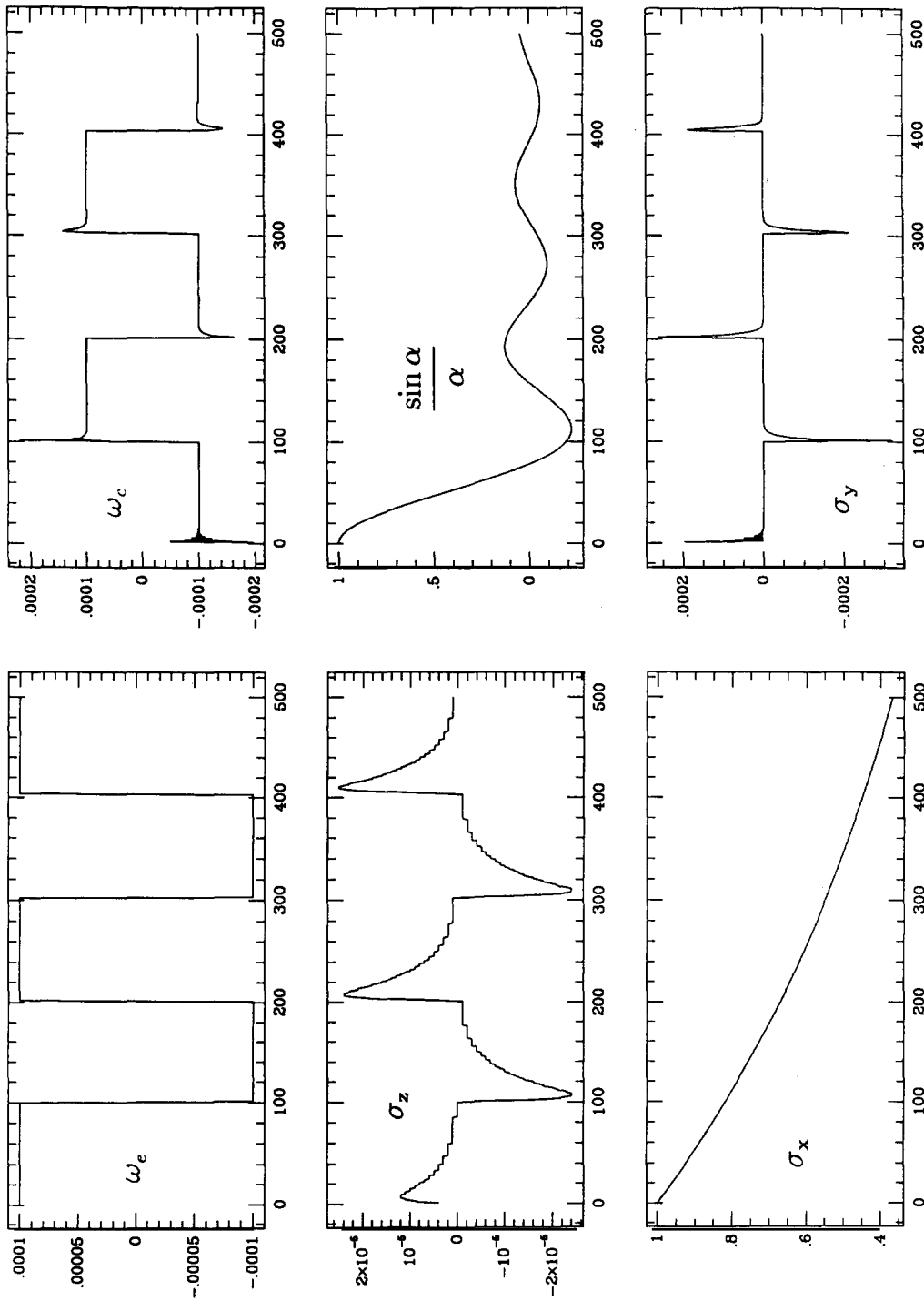


Fig. 10. Simulation including spin-dependent losses with $\omega_e = \pm 1 \times 10^{-4}$, reversed every 50 s. The loop is initially underdamped but becomes overdamped due to the gain reduction from neutron losses. The $\sin \alpha/\alpha$ reduction factor is shown to indicate the loss of sensitivity expected when feedback is not used; such a reduction is absent from the correction signal ω_c . Also, the component of σ_z due to the finite loop response time decays faster than σ_x ; this is due to spin-dependent losses.

over a 1000 s measurement interval), as shown in fig. 10. There is some dead time for one must wait approximately τ_L between reversals, and the field cannot be switched instantaneously, but we expect this to result in no more than a 10% loss in sensitivity.

5.6. Effects of offsets in the first-harmonic signal

Voltage offset in the first-harmonic phase-detector output leads to additional time dependent shifts in ω_z . If we include the offset as a constant voltage ε added to the output of the first-harmonic detector, the feedback keeps the sum

$$\langle s_y \rangle + \varepsilon = 0 . \quad (5.42)$$

The spin precesses in the applied magnetic field according to (neglecting losses or the spin dependence of $\text{Im } A$)

$$ds/dt = s \times B , \quad B = A\hat{x} + \omega_z\hat{z} , \quad (5.43a, b)$$

where A is constant and ω_z is determined by the feedback necessary to satisfy eq. (5.42). Expanding eq. (5.43a), using $s_y = \varepsilon$, a constant, we obtain the following equations:

$$\dot{s}_x = \varepsilon\omega_z , \quad \dot{s}_y = 0 = -s_x\omega_z + s_zA , \quad \dot{s}_z = -\varepsilon A . \quad (5.44a, b, c)$$

The last of these equations can be readily solved,

$$s_z = -\varepsilon A t . \quad (5.45)$$

The first two can be combined yielding

$$\varepsilon A s_z = s_x \dot{s}_x , \quad (5.46)$$

which leads to

$$-\varepsilon^2 A^2 t = s_x \dot{s}_x . \quad (5.47)$$

The exact solution of this equation is

$$s_x = \sqrt{1 - (\beta t)^2} , \quad \beta = \varepsilon A . \quad (5.48)$$

We thus obtain, from eq. (5.44a)

$$\omega_z = -\varepsilon A^2 t / \sqrt{1 - (\beta t)^2} \approx -\varepsilon A^2 t . \quad (5.49)$$

The approximate result can be obtained from eqs. (5.44b) and (5.45) directly by assuming $s_x = 1$. This result is unmodified in the presence of spin-independent losses, however, an additional time dependence is introduced if the neutron polarization varies with time, but this is expected to be a relatively weak effect.

This source of spurious shift can be kept small in a well-designed system. In addition, reversal of the electric field as described in the last section provides an additional discrimination against this effect.

6. Noise analysis

6.1. Model of the system for noise analysis

The determination of the signal-to-noise and hence the ultimate sensitivity to the neutron EDM is simplest in the context of feedback system analysis as described in section 5.4. A block diagram of a possible scheme is shown in fig. 7 and follows standard phaselock techniques.

Although the scintillation signal decays in time due to UCN loss, over a sufficiently short interval, the feedback system responds as a true phase-locked loop (PLL) [Gardner 1979]; that is, the first harmonic of the modulation signal depends on the average angle between the ^3He and UCN spins which is given by $\int \omega_e(t) dt$, and hence its Laplace transform is

$$V_1(t) = V_0 \int \omega_e(t) dt \Rightarrow V_1(s) = V_0 \omega_e(s)/s, \quad (6.1)$$

with V_0 depending slowly on time. That the form of the first harmonic-signal is given by eq. (6.1) can be readily seen by considering eq. (5.30) for T small: $\eta_+ - \eta_- \approx 2$ and $\eta_+ + \eta_- \approx \gamma T$ which implies that the first ω_e term of the rhs of eq. (5.30) increases as T^2 while the second term increases as T . We can thus neglect the first term since the feedback will be much faster than γ or Ω . To model the system, we need only consider the relative motion for very short times after the application of ω_e . The Laplace transform of a linear ramp is $1/s^2$ while that for a unit step of amplitude ω_e (at $T = 0$) is ω_e/s which when substituted in eq. (6.1) reproduces the expected $1/s^2$ dependence.

The signal-to-noise is most easily parameterized by the wall (and β) loss time $\tau_{w\beta}$; this is the one parameter in the system which cannot be easily changed. We thus need to optimize the following system parameters: the fill time T_f , the ^3He absorption rate τ_{He} , the modulation angle, and the duration of the measurement T_m , all as a function of P_3 , the ^3He polarization.

6.2. Initial polarization and UCN density

We start with a density of ^3He in the UCN storage volume giving a nominal loss rate for the spins antiparallel of $1/\tau_{\text{He}}$ with polarization P_3 and irradiate the entire volume with a 8.9 \AA neutron beam giving a total production rate of Φ_p UCN per unit volume. [Kilvington et al. 1987; Golub et al. 1991; Lamoreaux and Golub 1991]. The total number of the two UCN spin states depends on time as

$$\dot{N}_{\pm} = V\Phi_p/2 - N_{\pm}/\tau_{w\beta} - (1 \mp P_3)/\tau_{\text{He}}, \quad (6.2)$$

where \pm refers to the UCN spin parallel or antiparallel to the ^3He spin and V is the system volume. After collecting UCN for a time T_f , we find the initial UCN number and polarization (the loss of ^3He is negligible; it is also assumed that P_3 is constant throughout the

entire measurement),

$$N_{\pm}(T_f) = N_{\pm}^0 = (V\Phi_p/2\gamma_{\pm})[1 - \exp(-\gamma_{\pm} T_f)], \quad \gamma_{\pm} = 1/\tau_{w\beta} + (1 \mp P_3)/\tau_{\text{He}}. \quad (6.3)$$

The initial number of UCN is $N_0 = N_+^0 + N_-^0$.

6.3. Analysis of harmonically modulated dressing

For simplicity, we consider the case where the dressing parameter is harmonically modulated. In the presence of a nonzero EDM, the relative precession rate is given by

$$\omega = \omega_e + \omega_a \cos \omega_m t, \quad (6.4)$$

which gives a relative spin angle

$$\theta(t) = \int_0^t \omega dt = \int_0^t \omega_e(t) dt + (\omega_a/\omega_m) \cos \omega_m t. \quad (6.5)$$

The modulation index is defined as $\varepsilon = \omega_a/\omega_m$. The time dependence of the modulation signal is

$$\Phi(t) = [N(t)/\tau_{\text{He}}][1 - P_3 P_n(t) \cos \theta(t)], \quad (6.6)$$

where $N(t)$ is the total UCN density. Using the well-known Bessel function expansion in the case $\omega_e t \ll 1$ we find the average scintillation rate, first harmonic, and second harmonic (in ω_m)

$$\Phi_0(t) = [N(t)/\tau_{\text{He}}][1 - P_3 P_n(t) J_0(\varepsilon)], \quad (6.7)$$

$$\Phi_1(t) = 2 \frac{N(t)}{\tau_{\text{He}}} P_3 P_n(t) J_1(\varepsilon) \int_0^t \omega_e(t) dt, \quad \Phi_2(t) = 2 \frac{N(t)}{\tau_{\text{He}}} P_3 P_n(t) J_2(\varepsilon). \quad (6.8a, b)$$

It should also be noted that the UCN- ^3He system evolves under the average ^3He polarization which is $\langle P_3 \rangle = P_3 J_0(\varepsilon)$.

6.4. Evolution of the UCN polarization and density under modulated dressing

During the EDM measurement period, the 8.7 Å beam is turned off; however, the UCN density and polarization continue to change with decay rates, given by

$$\gamma'_{\pm} = 1/\tau_{w\beta} + (1 \mp \langle P_3 \rangle)/\tau_{\text{He}}. \quad (6.9)$$

The time evolution of N_{\pm} is then

$$N_{\pm}(t) = N_{\pm}^0 \exp(-\gamma'_{\pm} t). \quad (6.10)$$

The UCN polarization time dependence $P_n(t)$ and UCN density $N(t)$ are given by

$$P_n(t) = \frac{N_+(t) - N_-(t)}{N_+(t) + N_-(t)}, \quad N(t) = N_+(t) + N_-(t). \quad (6.11a, b)$$

Since $\gamma_+ < \gamma_-$, the UCN polarization continues to increase over the course of a measurement period.

6.5. Noise analysis in the feedback system

As discussed in section 6.1, over a short enough time interval, the feedback system introduced in section 5.4 behaves as a true PLL. This is evident from eq. (6.8a) where the first-harmonic signal increases linearly in time for constant ω_e ; this signal is proportional to the angle between the spins and hence is exactly analogous to the output of the phase detector in a PLL. Following standard system analysis, and as given in eq. (6.1), we introduce the Laplace transform to describe the response of the system to a unit step in ω_e ;

$$\mathcal{L}(\Phi_1) = \alpha_1/s = \mathcal{L}_1(s), \quad \alpha_1 = \alpha_1(t) = 2N(t)P_3P_n(t)J_1(\epsilon)/\tau_{\text{He}}, \quad (6.12)$$

where α_1 is time-dependent but varies much more slowly than the loop response time. For the loop analysis which involves time intervals short enough so that α_1 does not vary appreciably, we will take α_1 as a constant; however, we then consider the system gain adiabatically varying over the course of a measurement and will take the average system noise (over the measurement time), which depends on the gain, as the uncertainty in the EDM measurement.

As already mentioned, fig. 7 shows an integral plus proportional feedback system. For noise analysis, it is convenient to look at the response of the output from the first filter which has response

$$\mathcal{L}_2(s) = \beta + \alpha/s, \quad (6.13)$$

where α^{-1} is the integrator time constant and β the proportional component. The system response to a unit step of height ω_e at point A in fig. 7 is

$$\lim_{t \rightarrow \infty} V_{\text{out}}(t) = \lim_{s \rightarrow 0} s \left(H(s) \frac{\omega_e}{s} \right) = \lim_{s \rightarrow 0} \left(\omega_e \frac{\kappa \mathcal{L}_1(s) \mathcal{L}_2(s)}{1 + \kappa \mathcal{L}_1(s) \mathcal{L}_2(s)} \right) = \omega_e, \quad (6.14)$$

where an arbitrary scale factor relates *volts* to *Hertz* (gain of the voltage controlled oscillator; this factor can be absorbed in κ). At sufficiently low frequencies (less than the loop natural frequency) the loop tracks the input variations exactly.

The loop response for harmonic inputs is given by $H(i\omega)$. In particular, for a harmonic input at point B, the output response is given by

$$V_{\text{out}} = V_{\text{in}} i\omega H(i\omega)/\alpha_1 \approx i\omega/\alpha_1, \quad (6.15)$$

for sufficiently small ω .

Shot noise due to the average scintillation rate adds noise to the system at point B. The variation in scintillation rate in a time T is

$$\delta\Phi_0 = \sqrt{\Phi_0/T}, \quad (6.16)$$

or, using angular-frequency bandwidth to specify the time interval ($\delta\omega = \pi/T$), we obtain the mean-square fluctuation per unit bandwidth,

$$n_0 = \Phi_0/\pi, \quad (6.17)$$

since shot noise is white. The fluctuations in V_{out} are then

$$V_{\text{out}}^2 = n_0\omega^2/\alpha_1^2 \quad (6.18)$$

per unit bandwidth.

As proposed in section 5.5, the electric field will be modulated during the course of a measurement. We assume for now that this modulation is square; if the modulation frequency is much less than the loop natural frequency, the output voltage will be $V_{\text{out}}(t) = \pm\omega_e$ as in eq. (6.14) with a reversal rate of T_0^{-1} . The mean-square average of this is ω_e^2 ; the uncertainty in the measurement of ω_e is then given by the ratio of eq. (6.18) to the mean-square modulation deviation for unit ω_e ,

$$(\delta\omega_e)^2 = n_0\omega^2/\alpha_1^2 \quad (6.19)$$

per unit bandwidth. This signal is averaged for a time T_0 (for each modulation direction). We can model this averaging as a filter which has unit response for $\omega \leq \pi/T_0 = \omega_0$ and passes no signal of higher frequency. In that case, the variance in the output is

$$\sigma^2 = \int_0^{\omega_0} d\omega n_0\omega^2/\alpha_1^2 = \frac{1}{3}n_0\omega_0^3/\alpha_1^2. \quad (6.20)$$

Since n_0 and α_1 are slowly varying functions of time, the system sensitivity is given by the average variance over the entire measurement period as discussed previously,

$$\langle\sigma^2\rangle = (1/T_m) \int_0^{T_m} \sigma^2(t) dt. \quad (6.21)$$

Over the entire measurement period, we can perform $T_m/2T_0$ uncorrelated measurements ($T_m \gg T_0$), where the EDM is given by the difference in subsequent field directions [the variance per EDM measurement is thus twice that given in eq. (6.21)]. Furthermore, over a long period $T \gg T_m$ we can perform $T/(T_m + T_f)$ measurements (where T_f is the fill time). The system sensitivity

(in time T) is

$$\begin{aligned} (\Delta\omega_e)^2 &= 2 \frac{T_m + T_f}{T} \frac{2T_0}{T_m} \langle \sigma^2 \rangle = 2 \frac{T_m + T_f}{T} \frac{2T_0}{T_m} \frac{1}{T_m} \int_0^{T_m} \frac{1}{3} \frac{\Phi_0(t)}{\pi} \frac{\omega_0^3}{\alpha_1(t)^2} dt \\ &= \frac{4\pi^2}{3} \frac{T_m + T_f}{T} \frac{1}{T_m^2} \frac{1}{T_0^2} \int_0^{T_m} \frac{\Phi_0(t)}{\alpha_1(t)^2} dt. \end{aligned} \quad (6.22)$$

We must minimize $\Delta\omega_e$ with respect to T_m , T_f , τ_{He} , and the modulation index ε , given $\tau_{\text{w}\beta}$ and P_3 . We can scale all the times with $\tau_{\text{w}\beta}$ and let $T_0 = T_m/m$ with m an integer. The final frequency sensitivity is thus (in time T)

$$\Delta\omega_e = \sqrt{1/3} \pi m (1/\sqrt{T}) (1/\sqrt{\tau_{\text{w}\beta}}) (1/\sqrt{V\Phi_p \tau_{\text{w}\beta}}) f(\varepsilon, T_m, T_f, \tau_{\text{He}}), \quad (6.23)$$

$$f(\varepsilon, T_m, T_f, \tau_{\text{He}}) = 2 \left(\frac{T_m + T_f}{T_m^4} \int_0^{T_m} \frac{\Phi_0(t)}{\alpha_1(t)^2} dt \right)^{1/2}, \quad (6.24)$$

where Φ_0 and α_1 have been divided by $V\Phi_p \tau_{\text{w}\beta}$. The minimum value of f as a function of P_3 is shown in fig. 11. Also plotted are the values of the parameters (divided by $\tau_{\text{w}\beta}$) which minimize f . The fill and measurement times are relatively constant as a function of P_3 with $T_f = 0.9\tau_{\text{w}\beta}$ and $T_m = 2\tau_{\text{w}\beta}$ so are not shown in fig. 11.

If we assume $P_3 = 0.95$ ($f \approx 2$) over the course of a measurement, the frequency uncertainty is

$$\Delta\omega_e = (2\pi m/\sqrt{3}) (1/\sqrt{\tau_{\text{w}\beta} T}) (1/\sqrt{\Phi_p \tau_{\text{w}\beta} V}), \quad (6.25)$$

giving an EDM uncertainty of

$$\sigma(d_n) = \hbar \Delta\omega_e / 4EJ_0(x_c). \quad (6.26)$$

This can be compared to the EDM uncertainty from the current EDM experiments using Ramsey's method of separated oscillatory fields (neglecting dead time due to filling and emptying times which might be as much as a factor of $\sqrt{3}$ in the Hg comagnetometer experiment),

$$\sigma(d'_n) = (\alpha' E' \sqrt{N'_0 \tau'_{\text{w}\beta} T})^{-1}, \quad (6.27)$$

where $\alpha' \approx 0.65$ is the fringe visibility and, in the present UCN experiment, is coincidentally approximately equal to $J_0(x_c) = 0.65$.

There are several important differences between these two methods. First, in the new technique, the final uncertainty scales as $1/\tau_{\text{w}\beta}$ as opposed to $1/\sqrt{\tau_{\text{w}\beta}}$. This is because for the new technique both the initial density and frequency uncertainty per measurement depend on the system UCN loss time. The new technique also has a reduction in sensitivity because the effective coherence time is reduced by relaxation from the ^3He . The most important reduction in sensitivity comes from the

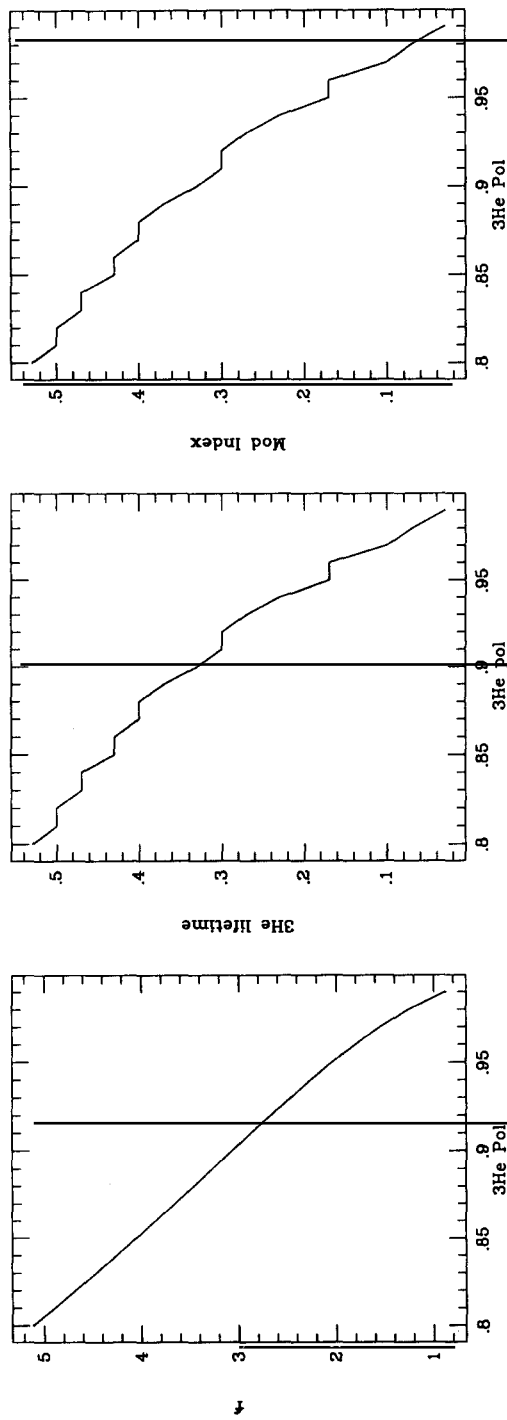


Fig. 11. The sensitivity factor f as a function of ^3He polarization, and the values of $\tau_{^3\text{He}}$ and modulation index ϵ which minimize f at the given ^3He polarization.

necessity of reversing the electric field over the course of a measurement; this gives the factor m which for a practical experiment must be at least 4. If we take $m = 4$, the ratio of sensitivity for the two methods is

$$\eta = \frac{\sigma(d'_n)}{\sigma(d_n)} = \frac{E}{E'} \frac{\sqrt{N_0}}{\sqrt{N'_0}} \frac{\sqrt{\tau_{w\beta}}}{\sqrt{\tau'_{w\beta}}} \frac{\sqrt{3}}{2\pi}, \quad N_0 = \Phi_p \tau_{w\beta} V, \quad J_0(x_c) = \alpha'. \quad (6.28)$$

As discussed in section 3, we anticipate a factor of 5 increase in electric field. Also anticipated is an increase in wall loss time from 100 s in the present experiments to 500 s. The present UCN density is about 2 cm^{-3} ; as discussed in section 3, a factor of 10 000 increase in N_0 is reasonable and requires $\Phi_p = 60 \text{ s}^{-1} \text{ cm}^{-3}$ with the wall loss $\tau_{w\beta} = 500 \text{ s}$ (assuming the experimental volumes are the same which is a quite reasonable expectation). With these, we get an increase in sensitivity of (including the $\sqrt{3}$ due to fill and empty dead time)

$$\eta = 534. \quad (6.29)$$

Using eqs. (6.25) and (6.26), we find using $\tau_{w\beta} = 500 \text{ s}$, $E = 50 \text{ kV/cm}$, $V = 2 \times 10^4 \text{ cm}^3$, and $\Phi_p = 40 \text{ cm}^{-3} \text{ s}^{-1}$, that the experimental sensitivity per unit time of running is

$$\sigma(d_n) = 8 \times 10^{-28} e \text{ cm} \quad \text{in one day}, \quad \sigma(d_n) = 4 \times 10^{-29} e \text{ cm} \quad \text{in one year}. \quad (6.30a, b)$$

That is over 2500 times more sensitive than the current experimental limit which was obtained in a similar length of time (but was limited by systematics), and is over 500 times more sensitive than the result anticipated in the Hg comagnetometer UCN experiment.

7. Some technical questions in regard to the proposed experiment

7.1. Overview of the experiment

We present in this section a very brief overview of some technical considerations and show that, in principle, the proposed experimental search for the neutron EDM is possible.

The various design considerations are all rather strongly coupled; for example, the choice of superfluid bath temperature affects the ^3He diffusion time, neutron-storage time, high-voltage properties, and scintillation properties, all of which suggest the lowest possible temperature ($\approx 0.5 \text{ K}$). However, for a heat-flush technique to be effective at removing depolarized ^3He from the superfluid bath, a rather higher temperature is required ($\approx 1 \text{ K}$) [McClintock 1978; Hendry and McClintock 1987].

This leads us to propose a system where the purification of the ^4He is performed in a separate chamber from where the EDM measurement takes place. The purification can then take place at a higher temperature; varying the temperature of the EDM storage vessel might introduce considerable dead time and would in addition make the high-sensitivity part of the apparatus unduly complicated. With the multichamber design, one is free to make the purification system arbitrarily slow and complicated; the only requirement is that on the order of 50 l of ultrapure ^4He is ready at the end of every approximately 1000 s measurement interval. It is clear that this would represent a considerable engineering feat, but it does not seem so daunting if we consider the effort

to build a single detector at CERN or Fermilab, and balance the cost with the expected increase in sensitivity for the neutron EDM search and the increase in our understanding of T violation which would accompany it.

Also, it might not be necessary to replace the ^3He after each measurement cycle; however, determining the final ^3He spin orientation so that the spin direction can be properly reoriented poses some technical difficulties.

Production of the UCN within the EDM chamber appears to be the simplest arrangement. This requires that the EDM chamber be irradiated with the cold neutron beam. Another possibility is to produce the UCN (in the presence of polarized ^3He) in a separate chamber, then transfer the UCN, polarized ^3He , and superfluid ^4He to the EDM chamber. There are advantages and disadvantages for both possibilities.

After an approximately 1000 s measurement interval, the superfluid is drained from the EDM chamber and sent to the purification facility. Most of the ^3He will leave with the superfluid since the diffusion rate into the cold ^4He gas above the superfluid is rather slow. By pumping on the EDM chamber, the remaining ^3He will be flushed out as the remaining superfluid film evaporates.

Some questions have already been addressed by Golub [1984] in relation to operation of such an experiment at a small reactor.

7.2. Operating temperature

The two primary considerations in choosing an operating temperature for the superfluid bath in the EDM chamber are the UCN upscattering rate and the ^3He diffusion time.

Golub et al. [1983] have shown that the UCN upscattering rate, when the number of phonons is small ($T < 0.7$ K), is determined by multiexcitation processes. Two-phonon processes dominate the upscattering and depend on temperature as T^7 . The UCN-upscattering lifetime is 2×10^3 s at 0.7 K; this temperature or lower is satisfactory from UCN storage-lifetime considerations.

A typical UCN velocity is 5 m/s. The correlation time associated with averaging the magnetic field over the storage volume is given by $\tau_c = L/v$, where L is the mean free path, which for a 20 l storage vessel (20 cm high by 35 cm diameter) is $L = 4V/S = 20$ cm, and $\tau_c = 0.04$ s. Ideally we would like to have the mean free path for the ^3He scattering by rotons, photons and ^3He on the same order as the dimensions of the storage chamber. However as we shall see this is neither possible nor necessary.

At temperatures where the mean free path is satisfactorily long ($T < 0.5$ K) and at the low ^3He concentrations of interest it is the ^3He -phonon collisions which dominate the ^3He diffusion. Husson and de Bruyn Ouboter [1983] (fig. 2 of that work) give the collision frequency for phonons with ^3He as $1/\tau_{\text{ph}} = 4.8 \times 10^{10} \cdot X T^4$, where X is the fractional ^3He concentration.

Then using $n_{\text{ph}}/\tau_{\text{ph}} = n_{\text{He}}/\tau_{\text{He}}$ we find $1/\tau_{\text{He}} = 4.8 \times 10^7 \cdot T^7 \text{ s}^{-1}$. Now the collisions counted by Husson and de Bruyn Ouboter [1983] are those effective in phonon transport, i.e., those collisions which change the phonon momentum by a significant amount. For elastic collisions, which dominate here, the momentum transfer for a phonon of momentum q , scattered through an angle θ_q ($\Delta q = 2q \sin \theta_q/2$), is equal to the momentum transfer to a ^3He atom with momentum p , scattered through an angle of θ_p ($\Delta p = 2p \sin \theta_p/2$), in the same collision. For every collision

$$p^2(1 - \cos \theta_p) = q^2(1 - \cos \theta_q), \quad (7.1)$$

therefore

$$\langle 1 - \cos \theta_p \rangle \simeq \langle 1 - \cos \theta_q \rangle \langle q \rangle^2 / \langle p \rangle^2 \simeq \langle 1 - \cos \theta_q \rangle T/10 . \quad (7.2)$$

Since the diffusion constant, D , is proportional to $\langle 1 - \cos \theta \rangle$ we can take the effective collision rate for ^3He

$$1/\tau_{\text{He}}^{\text{eff}} = 4.8 \times 10^6 \cdot T^8 , \quad (7.3)$$

and the diffusion constant for ^3He is

$$D = \frac{1}{3} \lambda_3 v_3 = \frac{1}{3} \langle v_3^2 \rangle \tau_{\text{He}} , \quad \lambda_3 = \langle v_3 \rangle \tau_{\text{He}} . \quad (7.4)$$

Thus the time t to diffuse a distance L is given by $L^2 = 2Dt$, and so

$$t = 3L^2/2v_3^2\tau_{\text{He}} = 0.28L^2T^7 = 120T^7 \text{ s for } L = 20 \text{ cm} \quad \text{or} \quad 1 \text{ s for } T = 0.5 \text{ K} . \quad (7.5)$$

The collision rate given in eq. (7.3) is about ten times smaller than that given by Ptukha [1961], and calculated by Khalatnikov and Zharkov [1957]. However, given the fact that there do not seem to be any direct measurements or reliable calculations in the relevant temperature and concentration regions, it seems the best estimate is that based on the above considerations. However, in the next section we will use a more conservative value of 5 s.

There is an unsolved problem concerning the motion of ^3He in dilute solutions although its ramifications at the low temperatures of interest here have not been investigated. Measurements of the thermal conductivity at low ^3He concentrations show the thermal conductivity approaching a constant rather than the expected $1/X$ behaviour. See Ferrel [1990] for a review, also Meyer et al. [1990] and Chiu and Lipa [1989], as well as appendix C for some additional comments.

Another important point to consider is the effects of unavoidable temperature gradients on the motion of the ^3He . In the case where the phonon density in the superfluid is high, a temperature gradient across the bottle will result in a significant ^3He concentration gradient, thereby affecting the volume average. At temperatures less than 0.7 K, such effects become rapidly insignificant.

7.3. Magnetic-field homogeneity requirements

If either the dressing or static magnetic-field gradients are too large, both the UCN and ^3He will suffer significant polarization loss over the storage interval due to phase decoherence (T_2 relaxation). Since the UCN velocity is anticipated to be higher than the ^3He diffusion time, the latter sets the time scale for field averaging (roughly 5 s as discussed above). It should be noted that such relaxation (T_2) does not occur during the UCN accumulation period of the measurement sequence (since the spin is not precessing during this period, the phase decoherence time is not important). Thus only spin flip (T_1) relaxation, which should be very long when the gradients are such that T_2 is long, occurs during this period. A reasonable value of T_2 is 10 000 s; the ^3He polarization would decrease by 10% over the measurement period, so the average is decreased by 5%, which should be acceptable.

Consider the case where the static magnetic field varies linearly over the storage vessel, with total change δB . The rms deviation of the static field is then $B_{\text{rms}} = \delta B/3$. Happer [1970] has shown that

the relaxation rate is given by

$$T_2^{-1} = \frac{2}{3} \tau_c (\gamma' B_{\text{rms}})^2, \quad \gamma' = \gamma J_0(x_c), \quad (7.6)$$

where γ' has units $\text{rad s}^{-1} (\text{mG})^{-1}$. With the values listed above, we find $\delta B \approx 1 \mu\text{G}$ which is about a factor of 10 smaller than in the Hg comagnetometer experiment where the storage vessel is of comparable dimension. Achieving the required homogeneity seems technically feasible.

For the dressing field, the requirements are slightly different. A gradient in the oscillating field gives a gradient in the Larmor frequency through the variation in the dressing parameter,

$$\omega = \gamma' B_0 = \gamma B_0 J_0(x_c), \quad \delta\omega = \gamma B_0 J_1(x_c) \delta x. \quad (7.7)$$

Since the frequency of the dressing field is well-defined and $x = \gamma B_{\text{rf}}/\omega_{\text{rf}} \approx x_c \approx 1$, we have

$$\delta x = \gamma \delta B_{\text{rf}}/\omega_{\text{rf}} \approx \delta B_{\text{rf}}/B_{\text{rf}}, \quad \delta\omega = \gamma B_0 J_1(x_c) \delta B_{\text{rf}}/B_{\text{rf}}. \quad (7.8)$$

Thus, T_2 is a result of the *relative* variation in B_{rf} , as opposed to the static field where it is the *absolute* variation. It is apparent that the dressing field-gradient relaxation rate depends on the static field magnitude; this implies working with the smallest possible applied static field. If we take $B_0 = 2 \text{ mG}$, and $J_1(x_c) \approx 0.5$, to achieve $T_2 = 10000 \text{ s}$ requires $\delta B_{\text{rf}}/B_{\text{rf}} < 1 \times 10^{-3}$. This is not too restrictive, however, the use of large-size conductive components in the EDM storage vessel or its environment will have to be avoided. Metal alloys become essentially insulators at low temperature so the electrodes, feedthroughs, and other components could be made from suitably chosen alloys (poor conductors can be used for the electrodes and high voltage supply lead since essentially no current flows). In addition, thin conductive films, if the frequency, ω_{rf} is not too high, can be used as heat shields, electrode coatings, etc., without disturbing the rf field. Larger conductive parts might be allowed if careful attention is paid to symmetry and placement.

7.4. High-voltage considerations

The insulating properties of liquid helium have been well studied, both for alternating electric fields (50 Hz) and dc. Fallou et al. [1969] have measured the dielectric strength of liquid He from 4.2 K to 1.5 K, at pressures up to 10 bar, and gap separations ranging from 0.1 to 10 mm, in uniform ac fields. They also measured the dielectric strength for non-uniform fields (point to plane) for both dc and ac. No significant changes as a function of pressure and temperature were found, although the breakdown voltage for a negative point was significantly lower than for a positive point. In the case of 50 Hz uniform fields, the dielectric strength was found to be 100 kV with a 10 mm gap, and the breakdown voltage increased linearly with gap size. They also studied the effect of a radioactive source (15 mCi of ^{192}Ir) placed in one of the electrodes which produced electrons through the Compton effect. The breakdown voltage was not lowered by this, however, the deviation between measurements was substantially reduced. The results of this and subsequent work show, for uniform fields, a dielectric strength of 30 kV/mm with a 1 mm gap [Fallou et al. 1969; 1970].

Gerhold [1972] found a dielectric strength of 40 kV/mm approximately constant for gaps varying from 0.1 to 1 mm. In these studies, it was found that contamination of the liquid He by oil or oil vapor made it useless as an insulator. Whether this is a surface or a volume effect remains to be studied. Such effects, if due to surface contamination, might restrict the types of wavelength

shifter used to detect the ultraviolet scintillations (see next section). However, it was found that contamination of the liquid He by frozen air particles did not alter the breakdown strength.

A further point to consider is that all of these measurements were performed between “free electrodes”—there was no insulating cylindrical tube separating the electrodes as is used for the EDM storage chamber. The effects of the presence of such dielectrics must be studied, as must the possible existence of a “gap effect”, i.e., a decrease in breakdown field with increased gap separation.

A reasonable voltage in view of generation and conduction to the EDM chamber is about 1 MV, which gives a factor of 5 increase in the electric field over the proposed Hg comagnetometer experiment, and a factor of 4 increase over the fields used at ILL and PNPI which led to the published results. A field order of 1 MV over 20 cm (5 kV/mm) is well below the observed dielectric strength of liquid He of 30–40 kV/mm.

It is interesting to note that for a fixed voltage, the EDM sensitivity scales as \sqrt{h} where h is the electrode separation (with fixed storage-chamber radius). This is because the final EDM sensitivity scales as

$$\sigma(d_n) \propto 1/E\sqrt{V} \propto 1/E\sqrt{h} \propto \sqrt{h}, \quad (7.9)$$

which implies that $h \rightarrow 0$ gives maximum sensitivity. However, the minimum h is determined by the dielectric strength. A safety factor of 6 as specified above is reasonable.

7.5. Scintillation detection

The scintillations produced by energetic particles in liquid helium was first studied by Thorndike and Shlaer [1959] and by Fleishman, Winbinder and Wu [1959]. Simmons and Perkins [1961] constructed a liquid He scintillation counter–polarimeter and studied a number of properties of the system. Their system employed a wavelength shifter (p, p'-diphenylstilbene deposited on the inside of the dewar) to convert the short-wavelength uv scintillation light to visible. They concluded that the light output, for α particles from a ^{239}Pu source, was comparable to a CsI(Tl) scintillator crystal. In addition, they show that there is little self-absorption by the liquid He of the scintillation light, and that the time structure of the pulses is similar to those of plastic scintillator (10 ns of ns rise and fall time). They also demonstrated that the scintillation light wavelength is less than 1600 Å.

Subsequent studies showed that the wavelength of the scintillation light is centered at about 800 Å, with a full width of about 200 Å [Stockton et al. 1970; Surko et al. 1970; Surko et al. 1969]. The spectral properties indicated that the light is generated by He_2 molecules. It was also observed that colloidal N_2 impurities decreased the uv light output.

The scintillation light from liquid He also has an infrared component [Dennis et al. 1969]. (In the presence of colloidal oxygen, visible light is produced [Jortner et al. 1964].) However, the intensity in these cases is much less than the uv scintillation at 800 Å.

Roberts and Hereford studied the effects of temperature and electric field on the uv scintillations produced by ^{210}Po α particles [Roberts and Hereford 1973; Hereford and Moss 1966]. They found that the total intensity decreased with temperature and electric field for temperatures greater than 0.8 K, but the total intensity increased with applied electric fields below this temperature. The effects of fields up to 13 kV/cm were studied. In these experiments, an organic dye POPOP was used as a wavelength shifter.

For our proposed neutron EDM experiment, it seems that detection of the uv scintillation via a wavelength shifter is the most promising scheme. A very small concentration of POPOP in

a deuterated carrier might be satisfactory. Deuterated polystyrene (DPS) as a wall coating material has already been shown to have excellent UCN storage properties and good vacuum high-voltage characteristics [Lamoreaux 1988]. The low-temperature and high-voltage properties of this material must be studied. Another possibility is to have frozen oxygen on the walls which is a good UCN storage material and might be a satisfactory wavelength shifter [Jortner et al. 1964].

The expected scintillation pulse width [Thorndike and Schlaer 1959] is less than $0.05 \mu\text{s}$ while the expected counting rate is $3 \times 10^4 \text{ cm}^3 \times 10^4 \text{ cm}^{-3} / 1000 \text{ s} = 6 \times 10^5 \text{ Hz}$. Thus the scintillations should be well resolved. The questions of background scintillations due to γ rays from the closely located reactor core and β rays from unavoidable neutron activation products in and around the storage vessel remain to be studied. Efficient collection of the scintillation light is also a difficult engineering problem, particularly if pulse-height discrimination is required to reject γ radiation effects.

7.6. Sources of cold neutrons

As discussed in section 3.2, we require a UCN production rate of $60/\text{cm}^3 \text{ s}$ which is about 30 times the rate obtained so far in a superthermal He source located at the end of a neutron guide. The required rate could be obtained at the ILL if the production vessel were located roughly 3 m from the cold source, with an unobstructed solid angle. It is unlikely that such an opening could be provided.

Golub [1984] has investigated the possibility of UCN production at small TRIGA-class reactors which typically have thermal power of 250 kW. With a liquid-nitrogen cooled moderator and a 500 s vessel lifetime, it is reasonable to expect a UCN density of 300 cm^{-3} . With a liquid-deuterium moderator, this might be increased by a factor of 10 which leads to a density only a factor of 7 lower than the design goal of $2 \times 10^4 \text{ UCN/cm}^3$. The issues of gamma background and heating at such a source are addressed in Golub [1984] and Golub and Böning [1981].

An existing source of cold neutrons with a flux over a large area is the Vertical Channel Universal Cold Source installed at the VVR-M Reactor of the Petersburg Nuclear Physics Institute, Gatchina, Russia [Altarev et al. 1986]. The liquid $\text{D}_2\text{-H}_2$ moderated source produces a Maxwell distribution with a temperature of 16.5 K, and a total integrated flux of $3 \times 10^{10} \text{ n/s}$, over an area $120 \times 40 \text{ mm}^2$, giving $\Phi = 6.3 \times 10^8 \text{ cm}^{-2} \text{ s}^{-1}$. Using eqs. (3.38) and (3.39) of Golub et al. [1991], we find a production rate

$$P = 1.4\Phi(E^*/T^2)\exp(-E^*/T) \times 10^{-7} \text{ UCN cm}^{-3} \text{ s}^{-1} = 1.9 \text{ cm}^{-3} \text{ s}^{-1}, \quad (7.10)$$

where $E^* = 11 \text{ K}$, $T = 16.5 \text{ K}$ and the numerical factor depends on the maximum UCN energy and hence on the wall material. However, the cold neutrons from this source are 90% polarized; the UCN produced by downscattering should maintain this polarization (there are no significant magnetic effects in the $n\text{-}^4\text{He}$ interaction). Thus, this is comparable to a production rate of $3.7 \text{ UCN cm}^{-3} \text{ s}^{-1}$, or a factor of 10 below that required. Also, the effective volume must be reduced by about a factor of 40 because of the reduced beam size over that anticipated earlier (from 35 cm diameter by 20 cm high to 12 cm diameter by 4 cm high).

However, the ultimate sensitivity should be about a factor of $\sqrt{2}$ higher due to an increased average UCN polarization. This represents a loss in sensitivity by a factor $(10 \times 40/2)^{1/2} = 15$. However, if the applied voltage is kept at 1 MV, the overall sensitivity loss is only a factor of 3.6, although the electric field would be 25 kV/mm – this is dangerously close to the breakdown field strength of liquid He and of possible materials such as SiO_2 which would be used as the insulating

cylinder. Also, the effect of such large fields on the properties of the scintillations is not known. In any case, this source would be ideal for an initial study of this complex system, and the rather small storage volume is an attractive simplification from a number of standpoints (magnetic gradients, quantity of liquid He required, efficient detection of scintillation light); even with the reduced volume and reduced flux, this source could be the basis for an experiment which would lead to a factor of 100 to 1000 (depending on attainable electric-field strength) improvement in the limit of the neutron EDM.

8. Conclusion

We have outlined an experimental technique to search for the neutron electric-dipole moment which offers the possibility of a 2000-fold improvement over existing experimental limits. Basically, the idea is to produce ultracold neutrons by downscattering 8.9 Å neutrons in superfluid He which is doped with a low concentration of polarized ^3He ; the ^3He serves as a UCN polarizer, analyzer and magnetometer. The effects of static magnetic fields are eliminated by use of a dressed magnetic-moment technique. The increase in sensitivity is due to a factor of 5 increase in electric-field strength, a factor of 5 increase in UCN storage time, and a factor of 10^4 increase in UCN density.

Such an improved limit is quite exciting in that this level is required to test whether the observed CP violation in K_0 decay can account for the baryon asymmetry in the universe. In addition, a factor of 10 to 100 increase in sensitivity over the current experimental limit will place rather strict bounds on the parameters of supersymmetric, multi-Higgs, and left-right symmetric models of CP violation. These models can readily accommodate a nonzero EDM between the present experimental limit and that anticipated for our proposed new technique. However, a failure to find a neutron EDM in this range will bring into question the veracity of these models [Weinberg 1992; He et al. 1989; Ellis 1989; Barr and Marciano 1989; Barr 1993].

There are some difficult technical questions to be answered in the development of an apparatus to exploit this technique, and we will begin with an experimental study of the diffusion of ^3He as described in appendix C. A more detailed discussion of the technical questions is forthcoming.

Acknowledgements

S.K.L. was supported by NSF grants PHY-8922274 and PHY-9100719. Helpful discussions with J.M. Pendlebury, R. Lipperheide and R. Bowley are gratefully acknowledged.

Appendix A. Mathematical operations on the Pauli matrices

Any 2×2 matrix can be written (taking out a constant as necessary) as

$$[M] = [1] + b[\sigma_i], \quad (\text{A.1})$$

where σ_i is some component of σ . Note $(\sigma_i)^2 = [1]$.

By use of the binomial theorem we can write

$$[M]^n = 1 + \binom{n}{1} b[\sigma_i] + \binom{n}{2} b^2[\sigma_i]^2 + \binom{n}{3} b^3[\sigma_i]^3 + \binom{n}{4} b^4[\sigma_i]^4 + \dots, \quad (\text{A.2})$$

or

$$[M]^n = 1 + \binom{n}{1} b[\sigma_i] + \binom{n}{2} b^2 + \binom{n}{3} b^3[\sigma_i] + \binom{n}{4} b^4 + \dots \quad (\text{A.3})$$

To sum the series we use the binomial theorem again to write

$$(1 \pm x)^n = 1 \pm \binom{n}{1} x + \binom{n}{2} x^2 \pm \binom{n}{3} x^3 + \binom{n}{4} x^4, \quad (\text{A.4})$$

so that

$$\begin{aligned} \frac{1}{2}[(1+x)^n + (1-x)^n] &= 1 + \binom{n}{2} x^2 + \binom{n}{4} x^4 + \dots, \\ \frac{1}{2}[(1+x)^n - (1-x)^n] &= \binom{n}{1} x + \binom{n}{3} x^3 + \dots \end{aligned} \quad (\text{A.5})$$

Thus

$$[M]^n = \frac{1}{2}[(1+b)^n + (1-b)^n] + [\sigma_i] \frac{1}{2}[(1+b)^n - (1-b)^n]. \quad (\text{A.6})$$

In our case $b \sim \tau = T/2n$ so we can use $\lim_{n \rightarrow \infty} (1 + a/n)^n = e^a$.

Appendix B. Quantum versus classical behaviour in the ^3He -UCN system

If we consider a system of ^3He and UCN spins precessing in a constant magnetic field taken along the z direction, the Hamiltonian written in the frame rotating with the ^3He precession frequency has the same form as (5.1). In the absence of a magnetic field ($\omega_z \rightarrow 0$) the eigenfunctions of the Hamiltonian are the eigenfunctions of $\sigma_n \cdot \sigma_3$. Assuming that the number of ^3He atoms in the system is much larger than the number of UCN we can take σ_3 as a classical field.

Taking σ_3 along the x axis, the eigenfunctions of the Hamiltonian are $|\pm\rangle_x$ with eigenvalues E_{\pm} giving two decaying eigenstates with decay times τ_{\pm}^{-1} :

$$E_{\pm} = \pm AP_3 - \frac{1}{2}i(1/\tau_0 \mp P_3/\tau_{\text{He}}), \quad 1/\tau_{\pm} = (1/\tau_0 \mp P_3/\tau_{\text{He}}). \quad (\text{B.1})$$

Just as in the $\text{K}_0\text{-}\bar{\text{K}}_0$ system, if we start in an arbitrary superposition of the two eigenstates the system evolves into the long-lived state ($\langle \sigma_n \rangle$ parallel to σ_3). Because of the difference in the real parts of the eigenvalues there will be oscillations during the evolution. After the long-lived state has been reached, the system can be restored to a superposition of the two eigenstates by switching σ_3 to a different direction, and the evolution towards the long-lived state will begin again.

Note that this is quite different than the behaviour of a system of classical spins which would decay with a single rate determined by the angle between the two spin species. What we have is a kind of Stern–Gerlach experiment on spatial quantization with the spin-dependent absorption serving as a state selector. However in the presence of a rapidly modulated external field as analyzed in section 5.2 we find exactly the classical behaviour. Equation (5.17) shows that if the system begins in an eigenstate it will decay with a single decay constant given by the average angle between the spins. Thus the rapid modulation produces a classical type decay behaviour. In the Stern–Gerlach experiment if we rapidly modulated the spin direction while the particles were in the high-gradient field region we would expect to see a deflection in the detector plane determined by the average of the spin direction in the gradient region. The situation can be understood on the basis of the “secular approximation” [Happer 1972; Barrat and Cohen–Tannoudji 1961].

In the case of a UCN interacting with the ^3He classical field, the mutual interaction Hamiltonian is

$$H = C\sigma_3 \cdot \sigma_n \pm \omega_z \quad (\text{B.2})$$

(C is a complex constant and ω_z is reversed with a frequency $\omega_m = 2\pi/\tau$) which, when the UCN spin direction (in the x – y plane, as described in section 5.2) is modulated at ω_m , can be separated into a slowly varying average term and a rapidly oscillating (at the modulation frequency and harmonics) term. In this case, the time evolution of a component of the density matrix is described by

$$\dot{\rho} = \left(A \langle \sigma_n \cdot \sigma_3 \rangle + \sum_k B_k \exp(ik\omega_m t) \right) \rho, \quad (\text{B.3})$$

where the average values of σ_n and σ_3 are slowly varying ($\ll \omega_m$), and $|A| \approx |B| \ll \omega_m$, and the B_k depend linearly on $\sigma_n \cdot \sigma_3 \leq 1$. We assume that the ^3He spin represents a fixed classical field, and assume that the B_k and A can be taken as constants. Then to first order in B/ω_m .

$$\rho(t) \approx e^{At} + B(\sin \omega_m t)/\omega_m, \quad (\text{B.4})$$

and we see the contribution from the oscillating terms suppressed.

The use of this formalism in the case of the Hamiltonian eq. (5.1) represents an interesting application of the secular approximation. In this case we have to work in the reference frame rotating at the instantaneous neutron Lamor frequency, so that the periodic excitation (the oscillating ^3He spin) satisfies the conditions for the application of the secular approximation as we discussed in section 5.3.

Appendix C. ^3He distribution in dilute ^3He – ^4He solutions: a new application of neutron beams

The ^3He in the UCN storage chamber will eventually become depolarized through T_2 relaxation processes which depend on inhomogeneities in the magnetic field. Thus, it will be necessary to periodically flush out the polarized ^3He and replace it with a new batch of freshly polarized ^3He . We intend to do this using the heat-flush technique [McClintock 1978; Hendry and McClintock 1987] which we have applied to purify the ^4He used in our previous work [Golub et al. 1983;

Kilvington et al. 1987]. In addition it may be necessary to use heat currents to insure an adequate motion of the ^3He so that the ^3He will see the same average value of the magnetic field as the UCN. For these reasons it will be necessary to study the motion and distribution of ^3He in very dilute solutions in the appropriate temperature range. This can be done using a new technique which we now describe and which, as we explain below, can have some interesting applications.

With a capture flux of $10^9 \text{ n cm}^{-2} \text{ s}^{-1}$ (easily obtainable at cold beams at the ILL) a 1 cm^2 beam will produce $10^{11} X \text{ captures s}^{-1} \text{ cm}^{-1}$, where X is the ^3He concentration. Thus if the background is low enough and if we can discriminate against γ -rays using the pulse height of the scintillations, we can detect extremely low ^3He concentrations and gradients in very dilute solutions, by scanning the neutron beam across the experimental cell.

This can have some interesting applications. For example, a significant deviation from the expected $1/X$ dependence of the thermal conductivity for $X < 10^{-5}$ has been experimentally observed. Two different models which have been proposed to explain this effect begin to differ markedly at $X < 10^{-7}$ [Ferrel 1990]. Present measurements extend to $X \approx 10^{-7}$. Measurements of the ^3He gradients by the neutron-beam scintillation technique are expected to yield results at much lower concentrations than existing measurements and thus would help to distinguish between the two models.

References

- Abragam, A. et al. 1972, C.R. Acad. Sci. B 274, 423.
 Abragam, A. and M. Goldman, 1982, Nuclear Magnetism: Order and Disorder (Oxford Univ. Press, Oxford).
 Abramowitz, M. and I.A. Stegun, 1972, Handbook of Mathematical Functions (Dover, Publ., New York).
 Altarev, I.S. et al., 1986, JETP Lett. 44, 344.
 Altarev, I.S. et al., 1992, Phys. Lett. 276, 242.
 Aminoff, C.G. et al., 1989, Rev. Phys. Appl. 24, 827.
 Barr, S.M., 1993, Int. J. Mod. Phys. A 8, 209.
 Barr, S.M. and W. Marciano, 1989, in: CP Violation, ed. C. Jarlskog (World Scientific, Singapore).
 Barrat, J.P. and C. Cohen-Tannoudji, 1961, J. Physique 22, 329; 22, 443.
 Casella, R., 1969, Phys. Rev. Lett. 22, 554.
 Chiu, T.C.P. and J.A. Lipa, 1989, Phys. Rev. B 40, 4306.
 Cohen-Tannoudji, C. and S. Haroche, 1969, J. Physique 30, 153.
 Coulter, K.P. et al., 1987, Tests of Time-Reversal Invariance in Neutron Physics, eds N.R. Robertson et al. (World Scientific, Singapore); Nucl. Instr. Meth. A 270 (1988) 90.
 Christenson, C.J., 1964, Phys. Rev. Lett. 13, 138.
 Dennis, W.S. et al., 1969, Phys. Rev. Lett. 23, 1083.
 Dirac, P.A.M., 1948, Phys. Rev. 74, 817.
 Dirac, P.A.M., 1949, Rev. Mod. Phys. 21, 392.
 Ellis, J., 1989, Nucl. Instrum. Methods Phys. Res. A 284, 33.
 Ellis, J. et al., 1981, Phys. Lett. B 99, 101.
 Fallou, B. et al., 1969, Supplement au Bulletin de l'Institut International du Froid, Commission 1, Londres (R.U.) 1969, Annexe 1969-1, p. 377.
 Fallou, B., J. Galand and B. Bouvier, 1970, Cryogenics 10, 142.
 Fermi, E. and L. Marshall, 1947, Phys. Rev. 71, 666.
 Fermi, E. and W.N. Zinn, 1946, Phys. Rev. 70, 103.
 Ferrel, R.A., 1990, Excitations in 2D and 3D Quantum Fluids, NATO Adv. Res. Workshop (Exeter).
 Fleishman, H., H. Einbinder and C.S. Wu, 1959, Rev. Sci. Instrum. 30, 1130.
 Foldy, L.L., 1945, Phys. Rev. 67, 107.
 Gardner, F.M., 1979, Phaselock Techniques, 2nd Ed. (Wiley, New York).
 Gerhold, J., 1972, Cryogenics 12, 370.
 Goldhaber, A.S. and W.P. Trower, 1990, Am. J. Phys. 58, 429.
 Golub, R. and J.M. Pendlebury, 1972, Contemp. Phys. 13, 519.
 Golub, R. and K. Böning, 1981, Report Jül-Spez 113/KfK3175, Part III-C, No. 3 (Jülich).
 Golub, R., 1983, J. Physique 44, L321.

- Golub, R., 1984, Nucl. Instrum. Methods Phys. Res. 226, 558.
- Golub, R., 1986, Sov. Phys. – Tech. Phys. 31, 945.
- Golub, R., 1987, in Proc. 18th Inter. Conf. on Low-Temperature Physics, Part 3: Invited Papers (Kyoto, Japan) p. 2073.
- Golub, R. et al., 1983, Z. Phys. B 51, 187, and references therein.
- Golub, R., D.J. Richardson and S.K. Lamoreaux, 1991, Ultracold Neutrons (Adam-Hilger, Bristol).
- Gordon, J.P., H.H. Zeiger and C.H. Townes, 1955, Phys. Rev. 99, 1264.
- Happer, W., 1970, Phys. Rev. B1, 2203.
- Happer, W., 1972, Rev. Mod. Phys. 44, 169 (Section II.E).
- He, X., B. McKellar and S. Pakvassa, 1988, Phys. Rev. Lett. 61, 1267.
- He, X., B. McKellar and S. Pakvassa, 1989, Int. J. Mod. Phys. A 4, 501.
- Hendry, P.C. and P.V.E. McClintock, 1987, Cryogenics 27, 131.
- Hereford, F.L. and F.E. Moss, 1966, Phys. Rev. 144, 204.
- Hunter, L.R., 1991, Science 252, 73.
- Husson, L.P.J. and R. de Bruyn Ouboter, 1983, Physica B 122, 201.
- Ignatovich, V.K., 1990, The Physics of Ultracold Neutrons (Oxford Univ. Press, Oxford).
- Jortner, J. et al., 1964, Phys. Rev. Lett. 12, 415.
- Khalatnikov, I.M. and V.N. Zharkov, 1957, Sov. Phys. – JETP 5, 9075.
- Kilvington, A.I. et al., 1987, Phys. Lett. A 125, 416.
- King, J.G. and J.R. Zacharias, 1956, Advances in Electronics and Electron Physics, Vol. VIII (1956).
- Koester, L., H. Rauch and H. Seymann, 1991, At. Nucl. Data Tables 49, 65.
- Lamoreaux, S.K., 1986, private communication to the ILL EDM group.
- Lamoreaux, S.K., 1988, Institut Laue–Langevin Internal Report 88LA01T, unpublished.
- Lamoreaux, S.K., 1989, Nucl. Instrum. Methods Phys. Res. A 284, 43.
- Lamoreaux, S.K., 1992, in: Proc. WEIN, Conf. on Weak and Electromagnetic Interactions in Nuclei (Dubna, CIS).
- Lamoreaux, S.K. and R. Golub, 1989, unpublished.
- Lamoreaux, S.K. and R. Golub, 1991, in: Massive Neutrinos and Tests of Fundamental Symmetries, eds O. Fackler, G. Fontaine and J. Tran Thanh Van (Editions Frontières, Gif-sur-Yvette, France).
- Lamoreaux, S.K. et al., 1987, Phys. Rev. Lett. 59, 2275.
- Landau, L.D., 1957, Nucl. Phys. 3, 127.
- Lanford, W. and R. Golub, 1977, Phys. Rev. Lett. 39, 1509.
- Lee, T.D. and C.N. Yang, 1956, Phys. Rev. 104, 254.
- Luders, G., 1957, Ann. Phys 2, 1.
- Luschikov, V.I. et al., 1968, Preprint P3-4127, JINR (Dubna, USSR).
- Luschikov, V.I. et al., 1969, Sov. Phys. – JETP Lett. 9, 23.
- Maier-Leibnitz, H. and T. Springer, 1963, J. Nucl. Energy 17, 217.
- Mampe, W., P. Ageron and R. Gähler, 1981, Z. Phys. B 45, 1.
- McClintock, P.V.E., 1978, Cryogenics 18, 201.
- Messiah, A., 1966, Quantum Mechanics (Wiley, New York).
- Meyer, H. et al., 1990, Excitations in 2D and 3D Quantum Fluids, in: NATO Adv. Res. Workshop (Exeter).
- Milner, R.G. et al., 1989, Nucl. Instrum. Methods Phys. Res. A 274, 56.
- Miranda, P.C., 1987, PhD Thesis, University of Sussex (Brighton, UK);
see also Miranda, P.C., 1988, J. Phys. D 21, 1326.
- Muskat, E.D., D. Dubbers and O. Schärpf, 1987, Phys. Rev. Lett. 58, 2047.
- Nachor, P.J. et al., 1982, J. Physique Lett. 43L, 525.
- Okun, L.B., 1969, Comments Nucl. Part. Phys. 3, 133.
- Passell, L. and R.I. Schermer, 1960, Phys. Rev. 150, 146.
- Pauli, W., 1955, Niels Bohr and the Development of Physics (Pergamon, New York) chap. 4.
- Pendlebury, J.M., 1992, Nucl. Phys. A 546, 359.
- Pendlebury, J.M. et al., 1984, Phys. Lett. B 136, 327.
- Polonsky, N. and C. Cohen-Tannoudji, 1965, J. Physique 26, 409.
- Ptukha, T.P., 1961, Sov. Phys. – JETP 13, 1112.
- Purcell, E.M. and N.F. Ramsey, 1950, Phys. Rev. 78, 807.
- Ramsey, N.F., 1956, Molecular Beams (Oxford Univ. Press, Oxford).
- Ramsey, N.F., 1958, Phys. Rev. 109, 225.
- Ramsey, N.F., 1978, Phys. Rep. 43, 409.
- Ramsey, N.F., 1982, Rep. Prog. Phys. 45, 95.
- Ramsey, N.F., 1984, Acta Phys. Hung. 55, 117.
- Roberts, H.A. and F.L. Hereford, 1973, Phys. Rev. A 7, 284.
- Sandars, P.G.H. and E. Lipworth, 1964, Phys. Rev. Lett. 13, 718.
- Schubert, K.R. et al., 1970, Phys. Lett. 313, 662.

- Scoles, G. ed., 1988, *Atomic and Molecular Beam Methods*, Vol. 1 (Oxford Univ. Press, Oxford).
- Sears, V.F., 1989, *Neutron Optics* (Oxford Univ. Press, Oxford).
- Shabilin, E.P., 1983, *Sov. Phys. – Usp.* 26, 297.
- Shapiro, F.L., 1968, *Sov. Phys. – Usp.* 11, 345.
- Simmons, J.E. and R.B. Perkins, 1961, *Rev. Sci. Instrum.* 32, 1173.
- Smith, J.H., 1951, PhD Thesis. Harvard University (Cambridge, MA.).
- Smith, J.H., E.M. Purcell and N.F. Ramsey, 1957, *Phys. Rev.* 108, 120.
- Smith, K.F. et al., 1990, *Phys. Lett. B* 234, 191.
- Steyerl, A., 1969, *Phys. Lett. B* 29, 33.
- Steyerl, A., 1977, Very low energy neutrons, in: *Springer Tracts in Modern Physics*, Vol. 80, Neutron Physics p. 57.
- Steyerl, A. et al., 1986, *Phys. Lett. A* 116, 347.
- Stockton, M. et al., 1970, *Phys. Rev. Lett.* 24, 654.
- Sumner, T.J., J.M. Pendlebury and K.F. Smith, 1987, *J. Phys. D* 20, 1095.
- Surko, C.M. et al., 1969, *Phys. Rev. Lett.* 23, 842.
- Surko, C.M. et al., 1970, *Phys. Rev. Lett.* 24, 657.
- Thompson, D., 1992, *J. Physique I* 2, 241.
- Thorndike, E.H. and W.J. Schlaer, 1959, *Rev. Sci. Instrum.* 30, 838.
- Vermeulen, G.A. and G. Frossati, 1987, *Cryogenics* 27, 139.
- Weinberg, S., 1992, in: *Proc. XXVI Inter. Conf. on High Energy Physics* (Dallas, Texas), summary talk.
- Wu, C.S. et al., 1957, *Phys. Rev.* 105, 1413.
- Zeldovich, Ya.B., 1959, *Sov. Phys. – JETP* 9, 1389.